Contrib Mineral Petrol (2016) 171:48
DOI 10.1007/s00410-016-1256-6

ORIGINAL PAPER

Inherited igneous zircons in jadeitite predate high-pressure metamorphism and jadeitite formation in the Jagua Clara serpentinite mélange of the Rio San Juan Complex (Dominican Republic)

Andreas Hertwig[1,2] · William C. McClelland[3] · Kouki Kitajima[4] · Hans-Peter Schertl[1] · Walter V. Maresch[1] · Klaus Stanek[5] · John W. Valley[4] · Sergey A. Sergeev[6,7]

Received: 19 October 2015 / Accepted: 28 March 2016 / Published online: 3 May 2016

Abstract This study utilizes zircon SIMS U–Pb dating, REE and trace-element analysis as well as oxygen isotope ratios of zircon to distinguish jadeite-rich rocks that formed by direct crystallization from a hydrous fluid from those that represent products of a metasomatic replacement process. Zircon was separated from a concordant jadeitite layer and its blueschist host, as well as from loose blocks of albite-jadeite rock and jadeitite that were all collected from the Jagua Clara serpentinite-matrix mélange in the northern Dominican Republic. In the concordant jadeitite layer, three groups of zircon domains were distinguished based on both age as well as geochemical and oxygen isotope values: age groups *old* (117.1 ± 0.9 Ma), *intermediate* (three dates: 90.6, 97.3, 106.0 Ma) and *young* (77.6 ± 1.3 Ma). Zircon populations from the blueschist host as well as the other three jadeite-rich samples generally match zircon domains of the *old* age group in age as well as geochemistry and oxygen isotope ratios. Moreover, these *older* zircon populations are indistinguishable from zircon typical of igneous oceanic crust and hence are probably inherited from igneous protoliths of the jadeite-rich rocks. Therefore, the results suggest that all investigated jadeite-rich rocks were formed by a metasomatic replacement process. The *younger* domains might signal actual ages of jadeitite formation, but there is no unequivocal proof for coeval zircon-jadeite growth.

Keywords Jadeitites · Zircon · Geochronology · Oxygen isotopes · Rio San Juan Complex

Communicated by Jochen Hoefs.

Electronic supplementary material The online version of this article (doi:10.1007/s00410-016-1256-6) contains supplementary material, which is available to authorized users.

✉ Andreas Hertwig
andreas.hertwig@rub.de

1 Institut für Geologie, Mineralogie und Geophysik, Ruhr-Universität Bochum, 44780 Bochum, Germany

2 Present Address: WiscSIMS, Department of Geoscience, University of Wisconsin, Madison, WI 53706-1692, USA

3 Department of Geoscience, University of Iowa, Iowa City, IA 52242, USA

4 WiscSIMS, Department of Geoscience, University of Wisconsin, Madison, WI 53706-1692, USA

5 Fakultät für Geowissenschaften, Geotechnik und Bergbau, TU Bergakademie Freiberg, 09599 Freiberg, Germany

6 Centre of Isotopic Research, Russian Geological Research Institute (VSEGEI), 199106 St.-Petersburg, Russia

7 Geological Faculty, St.-Petersburg State University, 199034 St.-Petersburg, Russia

Introduction

The term jadeitite designates a relatively rare rock type composed predominantly of the sodic clinopyroxene jadeite. Jadeitites are usually found in association with high-pressure metamorphic rocks in serpentinite-matrix mélanges worldwide that represent exhumed portions of the slab–mantle interface of fossil subduction zones. Currently, nineteen jadeitite occurrences have been described from serpentinite mélanges exposed in four Phanerozoic orogenic belts, including well-studied occurrences in the Caribbean island arc system (North and South of the Motagua Fault Zone, Guatemala; Sierra del Convento, Cuba; Rio San Juan Complex, Dominican Republic), the Circum-Pacific region (e.g., New Idria, USA; Osayama, Japan) as well as the Alpine-Himalayan (Monviso, Italy) and the

Caledonian orogens (e.g., Polar Urals, Russia) (see summary by Harlow et al. (2015)). Because the bulk-rock compositions of most jadeitites do not correspond to common igneous or sedimentary rocks, simple isochemical metamorphism cannot in general lead to jadeitite formation in subduction zones. At present, two jadeitite-forming end-member processes are being discussed. One possibility is that massive jadeitites may form by direct crystallization of jadeite from a high-pressure aqueous fluid ["vein precipitation" process (Yui et al. 2010) or "P-type jadeitites" ("fluid *p*recipitates" Tsujimori and Harlow 2012)]. In a second conceivable process, primary igneous minerals of a precursor rock are metasomatically altered via high-pressure aqueous fluids and finally replaced by jadeite ["metasomatic replacement" process (Yui et al. 2010) or "R-type jadeitites" ("*r*eplacement" Tsujimori and Harlow 2012)].

At present most authors appear to favor fluid precipitation (P-type jadeitite) as the dominant jadeitite-forming process (e.g., Tsujimori and Harlow 2012, and references therein), based on petrographic criteria initially summarized by Harlow and Sorensen (2005). These include the apparent lack of relict minerals in most jadeitites, the commonly observed oscillatory zoning pattern of jadeite crystals made visible by cathodoluminescence (CL) microscopy, and the often abundant fluid inclusions found in jadeite. Furthermore, Harlow (1994) and Harlow and Sorensen (2005) propose that the mass-transfer processes necessary during metasomatic replacement are complex and hence unlikely to have taken place. Unequivocal evidence indicating R-type genesis of jadeitites is rare, but the relict igneous clinopyroxene described by Compagnoni et al. (2007, 2012) in a jadeitite from the Monviso metaophiolite in Italy proves the metasomatic origin of this particular jadeitite sample. Additional evidence arguing in favor of R-type genesis is provided by Mori et al. (2011) and Yui et al. (2012), who identified presumably igneous inclusions in zircon from the Tone jadeitite in Japan.

Regardless of the mechanism of formation, fluids must play a major role in jadeitite genesis, and, hence, studying jadeitites can provide important information about fluid–rock interactions, fluid migration and fluid-mediated element transport in subduction zones (e.g., Harlow and Sorensen 2005). However, the overall extent of mass transport, especially whether material is removed from the site of jadeitite genesis by such a fluid, is strongly dependent on the nature of the jadeitite-forming process. Whereas the formation of P-type jadeitites can take place through an influx of Na–Al–Si–O–H-rich fluid, the transformation of plausible igneous protoliths such as oceanic plagiogranites to R-type jadeitites requires addition of Na and removal of Si, Ca, Mg and Fe during metasomatism (see discussion in Harlow 1994; Harlow et al. 2007). As a consequence, knowing the mode of formation of a jadeitite is indispensable before drawing any conclusions about the properties of the fluids involved.

The study of zircon has been shown to be essential for deducing the mode of formation of jadeitites, because zircon has the ability to retain initial isotopic and trace-element compositions, even after high-grade metamorphism (Valley 2003; Harley et al. 2007; Rubatto and Hermann 2007; Fu et al. 2010, 2012) or anatexis (Page et al. 2007b; Bowman et al. 2012) of the host rock. Identifying igneous (inherited) zircon in jadeitites would suggest a metasomatic origin of the jadeite-rich rock, whereas a population of exclusively hydrothermal zircon provides evidence for P-type jadeitite formation. Early geochronological studies on jadeitites argued in favor of a hydrothermal origin for zircon in jadeitites from Osayama in Japan (Tsujimori et al. 2005), and from Syros in Greece (Bröcker and Keasling 2006), based on inclusions of high-pressure minerals in zircon, which they interpreted as primary, and the general assumption of a P-type genesis for the investigated jadeitites. Fu et al. (2010) challenged this interpretation and utilized whole-rock and bulk-mineral (zircon, jadeite, albite) oxygen isotope ratios as well as ion microprobe spot analyses of $\delta^{18}O$ in zircon to demonstrate the probable igneous origin of most of the zircon from the Osayama, Syros and South Motagua (Guatemala) jadeitite samples. Further oxygen and hafnium isotope studies on zircon from the Syros jadeitite strengthened the interpretation that zircons predate jadeite for this particular locality (Fu et al. 2012). Subsequently, Flores et al. (2013) published a comprehensive in situ geochronological and geochemical study, including rare earth elements (REE), on zircon from jadeitites from North and South of the Motagua Fault Zone, questioning the conclusions of Fu et al. (2010) for the South Motagua jadeitites and suggesting a hydrothermal origin for all of the zircons. Yui et al. (2010, 2012) provided additional evidence for the hydrothermal origin of zircon from jadeitites from North of the Motagua Fault Zone.

Recently, Meng et al. (2016) described zoned zircon from a block of jadeitite from the Syum-Keu ultramafic complex of the Polar Urals, in which older cores of magmatic origin are overgrown by hydrothermally grown rims. Meng et al. (2016) interpret the magmatic zircon cores as relics of reworked subducted crustal protoliths. These older zircons were entrained by aqueous fluids and redeposited as P-type jadeitite elsewhere.

Additional geochronological and geochemical data (including REE patterns) are available for zircon from the Nishisonogi (Tone) jadeitite in Japan (both hydrothermal and igneous zircon, according to Mori et al. 2011; Yui et al. 2012), the Jade tract jadeitites in Myanmar (hydrothermal, Qiu et al. 2009; hydrothermal and igneous zircon, Shi et al. 2008; Yui et al. 2013) and the Polar Urals (hydrothermal and igneous zircon, Meng et al. 2011, 2016).

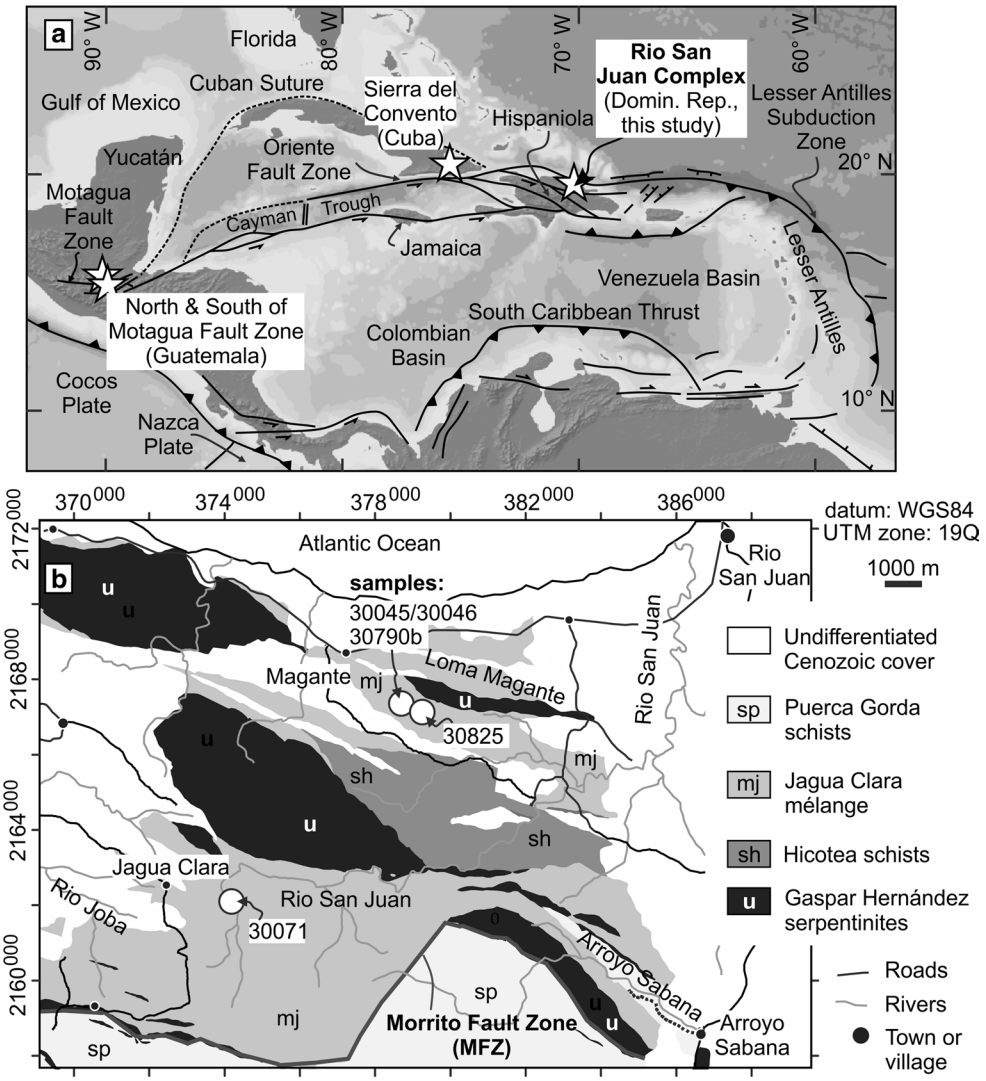

Fig. 1 Maps showing the location of the Rio San Juan Complex (RSJC), its principal geology, as well as sample localities. **a** Present tectonic setting of the Caribbean realm and location of documented jadeitite localities: North and South of Motagua Fault Zone (Harlow 1994; Harlow et al. 2011), Sierra del Convento (García-Casco et al. 2009; Cárdenas-Párraga et al. 2010, 2012). The RSJC is situated in the northern part of the Island of Hispaniola. Tectonic features modified from Pindell and Kennan (2009); base map utilizes global relief data of Amante and Eakins (2009). **b** Geological map of the northern part of the Rio San Juan Complex and sample localities. Map modified from Escuder-Viruete (2010). Escuder-Viruete et al. (2013b) interpret the Morrito Fault Zone to represent the suture zone between the Caribbean island arc and the paleocontinental margin of North America

Geochronological data, but not corresponding REE patterns, are available for zircon from the jadeitites of the Sierra del Convento in Cuba (hydrothermal zircon, Cárdenas-Párraga et al. 2012).

In order to clarify the mode of formation of the host rock, we have carried out a comprehensive ion microprobe study, including U–Pb age dating, trace-element and oxygen isotope analyses, of zircon from two jadeitites, an albite-jadeite rock and a blueschist from the Jagua Clara serpentinite mélange of the northern part of the Rio San Juan Complex (RSJC), Dominican Republic (Fig. 1). In addition to these four samples, we provide additional previously unpublished REE data (but no corresponding oxygen isotope analyses) for zircon from a phengite-rich jadeitite that has been described and dated by Schertl et al. (2012). In the RSJC, jadeitite can occur as concordant layers in lawsonite blueschist (Schertl et al. 2012), allowing direct comparison of zircon in the jadeitite with zircon in the enclosing blueschist host, and to relate jadeitite genesis to blueschist formation. The results presented here suggest an igneous origin for most of the analyzed zircon and, thus, point to a metasomatic (R-type) origin of these jadeite-rich rocks.

Geological setting and sample description

The northern Rio San Juan Complex (RSJC, Fig. 1a) is part of the exhumed forearc and accretionary prism of the Early Cretaceous to Paleogene Greater Antilles intra-oceanic subduction zone (Draper and Nagle 1991; Mann et al. 1991) and comprises greenschists and blueschists of the Hicotea, Puerca Gorda and El Guineal units as well as extensive bodies of the Gaspar Hernández serpentinites and the Jagua Clara serpentinite-matrix mélange (Draper and Nagle 1991; Escuder-Viruete et al. 2011, 2013a, b). Unlike the Gaspar Hernández serpentinites, the Jagua Clara serpentinite-matrix mélange contains tectonic blocks of a variety of

high-pressure metamorphic rocks including garnet-omphacite blueschists, jadeite-lawsonite blueschists, both sodium-amphibole-bearing and amphibole-free eclogites, granitic to trondhjemitic orthogneisses and minor metapelites, marbles, as well as various types of jadeite rocks (Krebs 2008; Krebs et al. 2008, 2011; Escuder-Viruete et al. 2011).

Maximum peak-metamorphic conditions in the Jagua Clara mélange of ~800 °C/26 kbar are recorded in eclogite blocks that follow clockwise as well as counterclockwise P–T paths (Krebs et al. 2011). Furthermore, Krebs (2008) and Krebs et al. (2011) distinguish three blueschist groups that differ systematically in their P–T paths (all clockwise): P–T paths of omphacite-free and jadeite-lawsonite blueschists follow "hair-pin"-like curves with P–T gradients of 13 and 6 °C/km, respectively. Omphacite-bearing blueschists show P–T paths similar to "open loops" and intermediate P–T gradients of 8 °C/km (Krebs et al. 2011). Jadeite-lawsonite blueschists experienced about 320–380 °C and 16–18 kbar, the lowest metamorphic grade reflected by high-pressure metamorphic rocks of the Jagua Clara mélange (Krebs 2008, Krebs et al. 2011). Escuder-Viruete and Pérez-Estaún (2013) studied the P–T evolution of high-pressure metamorphic rocks from several units of the RSJC and obtained peak-metamorphic conditions of 550–600 °C and 22–23 kbar on a counterclockwise P–T path for an eclogite block from the Jagua Clara mélange.

Combining P–T paths and geochronological data, Krebs et al. (2008, 2011) developed a three-stage model for the thermal evolution of the Greater Antilles subduction zone characterized by gradually steepening prograde P–T–t paths. A first "nascent" stage is distinguished by near-peak-metamorphic conditions of 750 °C/23 kbar at 103.6 ± 3.6 Ma (eclogite: Lu–Hf on garnet, omphacite, amphibole, epidote, bulk rock). The second "evolving" stage describes a cooling subduction zone allowing maximum metamorphic conditions of about 520 °C/17 kbar recorded at 80.3 ± 1.1 Ma in an omphacite-bearing blueschist (Rb–Sr on phengite, amphibole, bulk rock), followed by a third "mature stage" at about 62–72 Ma with peak conditions of <400 °C/16 kbar (jadeite-lawsonite blueschist: Ar–Ar on phengite; jadeite blueschist: Rb–Sr on phengite, amphibole, bulk rock) (Krebs et al. 2008, 2011). A sodium-amphibole-bearing eclogite and a lawsonite-bearing metatrondhjemite possess protolith ages of 139.1 ± 3.6 Ma (U–Pb TIMS on zircon, Krebs et al. 2008) and 94.7 ± 3.1 Ma (U–Pb TIMS on zircon, Krebs 2008), respectively. In order to study the deformational history of the RSJC, Escuder-Viruete et al. (2013a) performed U–Pb and Ar–Ar dating on phengite-bearing leucotonalite and trondhjemite sills collected from two localities in the Jagua Clara mélange. Based on field and petrographical observations as well as geochronology, Escuder-Viruete et al. (2013a) concluded that the tonalite sill intruded the mélange at 71.3 ± 0.7 Ma (U–Pb SHRIMP age) synchronous with a major retrograde, ductile shearing event in the Early Maastrichtian. Leucotonalite and trondhjemite sills are interpreted to represent crystallized subduction-related, "adakite-like" melts (Escuder-Viruete et al. 2013a).

Schertl et al. (2012) divided the jadeite rocks (excluding jadeite-rich blueschists) exposed in the northern RSJC, based on the absence or presence of quartz in the rock matrix, into a (matrix-) quartz-free and quartz-bearing rock suite, respectively. Both suites contain jadeitite s.str. (sensu stricto, >90 vol% jadeite, Harlow 1994) and jadeitite s.l. (sensu lato, >75 vol% jadeite), which in the case of the quartz-bearing suite may form concordant layers in blueschist—a rare association worldwide (Schertl et al. 2012). In addition, the usually albite-bearing matrix-quartz-free jadeite rocks comprise phengite-jadeite, omphacite-jadeite and jadeite-albite rocks. Jadeite rocks of the matrix-quartz-bearing suite include jadeite quartzites and jadeite-lawsonite quartzites (Schertl et al. 2012; Hertwig 2014). In addition to the concordant layers, the latter may also form discordant veins in blueschist, although both types have not been found together in the same sample. So far, zircon has never been observed in discordant veins. Hertwig (2014) deduced maximum P–T conditions for a jadeite-lawsonite quartzite layer within a jadeite blueschist of 350–450 °C and >10–12 kbar, in agreement with peak-metamorphic conditions inferred by Krebs et al. (2011) for jadeite (-lawsonite) blueschist blocks of the same area.

The main emphasis of this study is on four samples that originate from the Loma Magante area of the Jagua Clara mélange (Fig. 1b), roughly 2 km from the Atlantic coast. Zircon grains were separated from a concordant quartz-bearing jadeitite layer (sample 30046) and its blueschist host (30045), from an albite-jadeite rock (30790b) and a jadeitite block (30825). Samples 30046 and 30045 were taken from a single blueschist block ($2 \times 2 \times 1$ m^3), whereas samples 30790b and 30825 are from loose individual blocks (~1 m in diameter) collected at the northern ridge of Loma Magante. A fifth sample included here is a phengite-rich jadeitite (sample 30071; WGS84, UTM 19Q, 374008, 2162176) that was found as a boulder in the river bed of the Rio San Juan in the southern part of the Jagua Clara mélange approximately 10 km from the coast (Fig. 1b). The petrography of this sample, zircon textures and geochronological data have already been published and described elsewhere (Schertl et al. 2012).

The concordant quartz-bearing jadeitite layer (sample 30046; WGS84, UTM 19Q, 378297 2167456; Figs. 1b and 2) possesses an overall granoblastic texture and consists of jadeite (90 vol%, $Jd_{92}Di_7Hd_1$–$Jd_{99}Di_1$), quartz (5 vol%), glaucophane (3 vol%), calcite (1 vol%), phengite (1 vol%, Si ~ 3.50–3.65 apfu) and accessory apatite, titanite and zircon. The jadeite is inclusion-rich and usually subhedral to

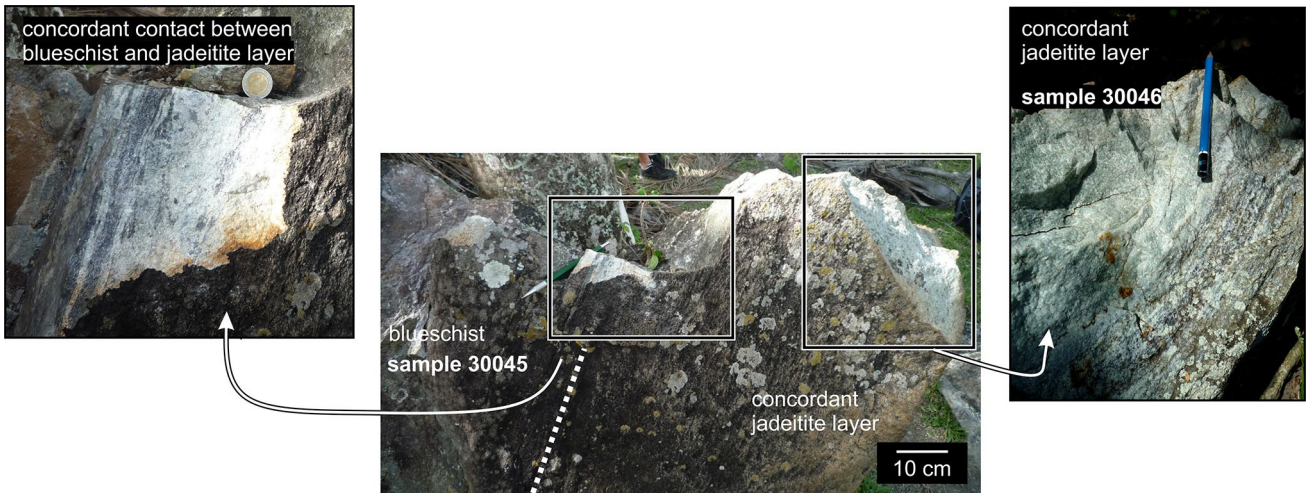

Fig. 2 Photographs showing a blueschist block (2 × 2 × 1 m^3) at the Loma Magante locality (UTM grid zone 19Q, WGS84, 378297 2167456) with a concordant jadeitite layer. Close-up photographs picture the contact between blueschist and jadeitite layer (*left*) as well as the jadeitite layer itself

anhedral; quartz is present as inclusions in jadeite and also occupies interstitial positions. Further information about the petrography and mineral chemistry of sample 30046 can be found in Schertl et al. (2012). The matrix of the blueschist host (30045) close to the contact with the jadeitite layer contains two generations of glaucophane (~70 vol%), inclusion-rich lawsonite (~20 vol%) and evenly distributed roundish aggregates of jadeitic clinopyroxene (~10 vol%, ~$Jd_{70–90}$). At the contact with the jadeitite layer, jadeite is intergrown with poikiloblastic lawsonite. Accessory minerals of the blueschist are phengite (Si ~ 3.50–3.65 apfu), titanite, apatite and zircon.

The strongly veined albite-jadeite rock (sample 30790b; WGS84, UTM 19Q, 378348 2167338; Fig. 1b) is mainly composed of inclusion-rich (quartz, calcite, albite) partly retrogressed jadeite (40 vol%, ~$Jd_{95}Di_2Hed_3$–$Jd_{99}Di_1$) as well as albite (30 vol%, an_1) and calcite (15 vol%), which are also the main constituents of the veinlets. Additional minerals are chlorite (5 vol%), sulfides (5 vol%, mainly pyrite with inclusions of quartz), epidote-group minerals (2 vol%, Fe^{3+} ~ 0.5–0.9 apfu) and titanite (2 vol%). An unusual feature for jadeite rocks of the RSJC is the presence of aegirine-augite (1 vol%, ~$Jd_{10}Aeg_{32}Di_{42}Hd_{16}$–$Jd_{10}Aeg_{38}Di_{42}Hd_{10}$) that forms mineral clusters together with chlorite, titanite and albite. Accessory phases are phengite (Si ~ 3.13–3.26 apfu), glaucophane and zircon.

The major mineral constituents of the faintly foliated jadeitite block (sample 30825; WGS84, UTM 19Q, 379601 2166998, Fig. 1b) are anhedral jadeite (75 vol%, ~$Jd_{82}Aeg_9Di_8Hd_1$), subhedral lawsonite (10 vol%) and chlorite (7 vol%). Minor constituents are phengite (4 vol%, Si ~ 3.15–3.40 apfu), epidote-group minerals (2 vol%, Fe^{3+} ~ 0.5 apfu), titanite (1 vol%) and, again an exceptional feature for the RSJC, paragonite (1 vol%, $Pg_{0.81–0.98}$). Albite ($An_{1–2}$) and zircon are accessory phases.

Analytical methods

The selected rock samples were disintegrated by application of high-voltage electric pulses using the "Selfrag Lab" laboratory equipment (SELFRAG AG, Switzerland) located at the Institute of Geology, TU Bergakademie Freiberg (TUBAF), Germany. Comprehensive descriptions of the underlying physical processes and their technical implications are given by Andres (2010) and van der Wielen et al. (2013). Utilizing the 80- to 250-µm grain fraction, zircon separation was achieved with the following standard gravimetric and magnetic techniques (according to the mineral separation protocol of the mineral separation laboratory of TUBAF, in processing sequence): wet shaking table concentrator (Wilfley table), Frantz Magnetic Separator, heavy liquid separation (step 1: bromoform, 2: methylene iodide) and, finally, hand picking of zircon grains.

For U–Pb, trace-element and oxygen isotope analysis, zircon grains were mounted in a 2.54-cm-diameter epoxy disk, together with zircon standards R33 (U–Pb isotopic composition) and KIM-5 (oxygen isotopes). The subsequent documentation of the zircon mount was performed by cathodoluminescence (CL) and reflected-light imaging. U–Pb dating and trace-element analyses were carried out in separate analytical sessions (data sets 1 and 2) using the SHRIMP-RG (sensitive high-resolution ion microprobe–reverse geometry) ion microprobe at the US Geological Survey–Stanford University Ion Probe Laboratory, CA, USA. Data set (1), provided in electronic supplementary

material 1 (ESM 1), comprises U–Pb isotopic compositions of zircon domains as well as a limited number of concurrently determined rare earth elements; data set (1) was used for age determination of zircon domains (geochronology session). Data set (2), provided in ESM 2, covers an extended number of trace elements, as well as analyses of Al, Ca, Si and Fe in order to screen for the negative effects of contamination by minute inclusions in zircon (trace-element session). The position of analysis spots was guided by CL textures of zircon that define domains within individual zircon grains.

U–Pb data were acquired using a spot size of 25–30 μm, utilizing the analytical routine outlined in Barth and Wooden (2006, 2010) and the program SQUID (Ludwig 2001) for data reduction. Concentration calibration of U was based on zircon standard Madagascar Green (MAD; 4196 ppm U; Barth and Wooden 2010). Isotopic ratios were calibrated by replicate analyses of zircon standard R33 (421 Ma, Black et al. 2004; Mattinson 2010). The $^{206}Pb/^{238}U$ isotopic ratios were corrected for common Pb using the ^{207}Pb method of Williams (1998); initial common Pb estimation was according to Stacey and Kramers (1975). Ages given are inverse-variance weighted mean $^{206}Pb/^{238}U$ ages with errors representing the 95 % confidence interval. The program Isoplot/Ex (Ludwig 2003, 2012) was used to draw Tera-Wasserburg diagrams.

Trace-element analysis followed analytical routine of Mazdab and Wooden (2006). Calibration of elemental concentrations used zircon standards CZ3 and MAD (Mazdab and Wooden 2006; Mazdab 2009). The routine for trace-element analysis simultaneous with U, Th and Pb included ^{89}Y, ^{139}La, ^{140}Ce, ^{146}Nd, ^{147}Sm, ^{153}Eu, ^{155}Gd, $^{163}Dy^{16}O$, $^{166}Er^{16}O$, $^{172}Yb^{16}O$, $^{90}Zr_2^{16}O$ and $^{180}Hf^{16}O$. Analysis for the extended trace-element suite used a spot size of 10 μm to acquire concentrations of ^{7}Li, ^{9}Be, ^{11}B, ^{19}F, ^{23}Na, ^{27}Al, ^{30}Si, ^{31}P, ^{39}K, ^{40}Ca, ^{45}Sc, ^{48}Ti, ^{49}Ti, ^{56}Fe, ^{89}Y, ^{93}Nb, $^{94}Zr^{1}H$, ^{96}Zr, ^{139}La, ^{140}Ce, ^{146}Nd, ^{147}Sm, ^{153}Eu, ^{155}Gd, ^{165}Ho, $^{159}Tb^{16}O$, $^{163}Dy^{16}O$, $^{166}Er^{16}O$, $^{169}Tm^{16}O$, $^{172}Yb^{16}O$, $^{175}Lu^{16}O$, $^{90}Zr_2^{16}O$, $^{180}Hf^{16}O$, ^{206}Pb, $^{232}Th^{16}O$ and $^{238}U^{16}O$. Estimated errors of element concentrations, based on replicate analyses of the MAD standard, are less than 5 % for P, Sc, Ti, Y, Th, U, Ho–Lu, between 5 and 10 % for Nd–Gd and ~30 % for La.

Chondrite-normalized REE values are indicated by a subscript (N) and were obtained using the chondritic abundances tabulated by Anders and Grevesse (1989), multiplied by a factor of 1.36 (Korotev 1996). When data set (1) was used to plot REE patterns (sample 30046 only), values for Pm, Tb, Ho, Tm and Lu were interpolated; when data set (2) was used, Pm was interpolated. In both data sets Pr was calculated and defined as $Pr_{(N)} = La_{(N)}^{1/3} \times Nd_{(N)}^{2/3}$. The Eu anomaly was calculated as $Eu/Eu^* = Eu_{(N)}/(Sm_{(N)} \times Gd_{(N)})^{0.5}$, and the Ce anomaly as $Ce/Ce^* = Ce_{(N)}/(La_{(N)} \times Pr_{(N)})^{0.5}$.

Oxygen isotope analyses were carried out at the Wisc-SIMS Laboratory (University of Wisconsin-Madison) utilizing the Cameca IMS-1280 ion microprobe and following analytical procedures described in Kita et al. (2009) and Valley and Kita (2009). The primary Cs^+ beam (1.7–1.9 nA) was focused on the zircon mount surface to provide an analysis spot of 12 μm in diameter. Special care was taken to analyze the same zircon domains that had been previously dated and analyzed for trace elements. Previous analysis pits were ground away, and the grains repolished before oxygen isotope analysis. In two analytical sessions, a total of 294 analyses were made, including 95 standard analyses. The KIM-5 zircon oxygen isotope standard ($\delta^{18}O(Zrn) = 5.09$ ‰ VSMOW, Valley 2003) was applied to calibrate the $\delta^{18}O(Zrn)_{VSMOW}$ of the unknowns. One set of usually 10–12 unknowns was bracketed by two sets of standard analyses (4 spot analyses before and 4 after the unknowns, see Fig. 3) to correct for instrumental bias and drift. The precision of the analyses, expressed as ±2 SD, is defined by the external precision of the standard analyses (spot-to-spot analyses on KIM-5). Oxygen isotope data are tabulated in ESM 4.

Prior to oxygen isotope analysis, CL and secondary electron (SE) images of zircon grains were made by SEM to document the grain surface after SHRIMP-RG analysis and to guide oxygen isotope measurements. Thereafter, the sample mount was polished by hand to remove existing pits and relief and flatten the surface. After oxygen isotope analysis, individual zircon grains were imaged by color CL and SE methods to document the zircon mount after SHRIMP-RG and IMS-1280 analyses and to evaluate whether analysis spots had hit small fissures and inclusions that might have caused contamination of analyses. Color CL images with locations of ion microprobe analysis pits are shown in ESM 5.

REE data of zircon from the phengite-rich jadeitite (sample 30071, see ESM 3) were acquired using the SHRIMP-II instrument hosted at the Centre of Isotopic Research of the VSEGEI in St. Petersburg.

Results

Zircon morphology, SIMS dating and geochemical composition of zircon

The concordant layer of jadeitite (30046)

Zircon grains from the concordant jadeitite layer (100–200 μm length, aspect ratio 1:2 to 1:3) constitute two heterogeneous morphological subpopulations. One population

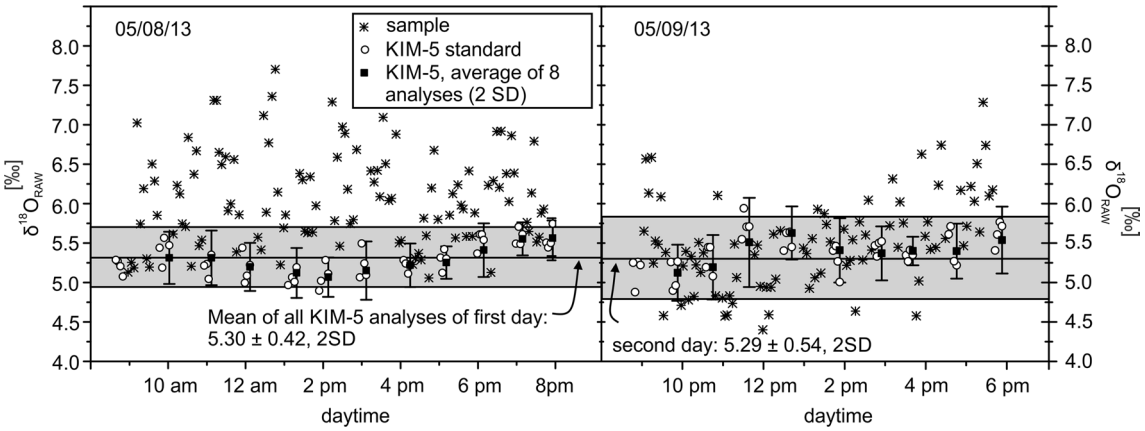

Fig. 3 Oxygen isotope analyses of zircon unknowns (sample analyses) and zircon standard (KIM-5, uncorrected raw data) attained during two analytical sessions on May 8 and 9, 2013 at the WiscSIMS Laboratory (University of Wisconsin-Madison). *Error bars* (2 SD, external precision) defined by 8 standard analyses bracketing the unknowns. Complete oxygen isotope data are presented in ESM 4

contains mainly anhedral to subhedral grains with partly resorbed shapes (e.g., grains no. 1, 2, 3, 8, 16 in Fig. 4a), while a second population possesses subhedral to even euhedral crystal shapes (e.g., no. 9, 10, 12, 18). As revealed by CL imaging, zircon grains show a variety of internal textures such as weakly to well-developed oscillatory zoning patterns (no. 1, 3, 4, 10, 12, 15, 18), crystal core–rim relationships (no. 9, 12), irregular zoning patterns (no. 5, 14, 17) or no obvious zoning textures at all (no. 16). Some grains show microveining (no. 3, 19) or have been affected by late-stage alteration processes at crystal rims (no. 9, 10, 18). According to their spatial relationship, zircon domains were categorized into core, mantle and rim during the SIMS sessions. Most core domains are CL-dark (low CL intensity, see grains no. 1, 3, 4, 8, 9) and possess variably sized CL-bright rims. The weakly oscillatory zoned grain no. 10 is uniformly CL bright; grains no. 17 and 18 are composed of CL-bright domains of varying CL intensities. Moderately luminescent domains can occupy a textural position between crystal cores and rims (no. 4, 11), constitute the rim itself (no. 7) or form individual, only slightly or irregularly zoned grains (no. 14, 16). In general, zircon grains are poor in mineral inclusions, and, when present, mineral inclusions accumulate close to the rim along cracks (e.g., upper right corner of grain no. 9). In zircon from the concordant jadeitite layer, apatite and an unspecified Ca–Fe–Si–Al phase are the only possibly primary mineral inclusions that were entrapped during the growth of zircon.

Zircon domains from the concordant jadeitite yield $^{206}Pb/^{238}U$ dates from about 70–118 Ma (Table 1) that can be pooled into three different age groups. A first age group is defined by analyses of three CL dark (no. 1, 3, 8) and three domains of varying CL intensities (no. 5, 6, 14). These analyses constitute the *old* age group and give a weighted mean $^{206}Pb/^{238}U$ age of 117.1 ± 0.9 Ma ($n = 6$, MSWD = 1.2, see Fig. 4b) or a concordia age of 117.2 ± 0.4 Ma. Eight analyses define the *young* age group that comprise 5 concordant (concordia age: 78.5 ± 0.7 Ma) and 3 discordant analyses that, when treated as a coherent age group, give a weighted mean age of 77.6 ± 1.3 Ma ($n = 8$, MSWD = 2.0). The *intermediate* age group consists of three slightly discordant analyses with $^{206}Pb/^{238}U$ dates between 90.0 ± 1.4 Ma and 106.0 ± 1.6 Ma. Zircon grain no. 13 yields an estimated $^{206}Pb/^{238}U$ date of roughly 940 Ma and is excluded from further discussion.

Depending on the ages of the respective zircon domains, their chondrite-normalized REE patterns (Fig. 5a, b) exhibit systematic differences in their overall shape. Three basic features of the REE patterns are illustrated in Fig. 5a, b: First, zircon domains of all age groups have a positive Ce anomaly that is most prominent in zircon from the *old* and *intermediate* age groups (*old* and *intermediate*: Ce/Ce* = 48–371, $n = 9$) and less developed in *young* domains (Ce/Ce* = 1.2–10.7, $n = 8$). Second, analyses of *young* domains show a slightly positive Eu anomaly (Eu/Eu* = 1.38–5.89, $n = 8$), which is in contrast to the negative Eu anomaly (Eu/Eu* = 0.41–0.76, $n = 6$) of *old* domains. Third, domains of the *young* age group are more strongly enriched in heavy rare earth elements (HREE, $Yb_{(N)}/Gd_{(N)}$ = 112–899, $n = 8$; Fig. 5d) than domains of the *old* age group ($Yb_{(N)}/Gd_{(N)}$ = 28–36, $n = 6$); analyses of domains of the *intermediate* age group show flat HREE patterns ($Yb_{(N)}/Gd_{(N)} = 2–7$, $n = 3$).

Th/U ratios vary systematically depending on the age group of the zircon domains (Fig. 5e). *Young* zircon domains usually have Th/U ratios of less than 0.03, whereas *old* domains possess higher ratios between 0.1 and 0.4; domains of the *intermediate* age group show the

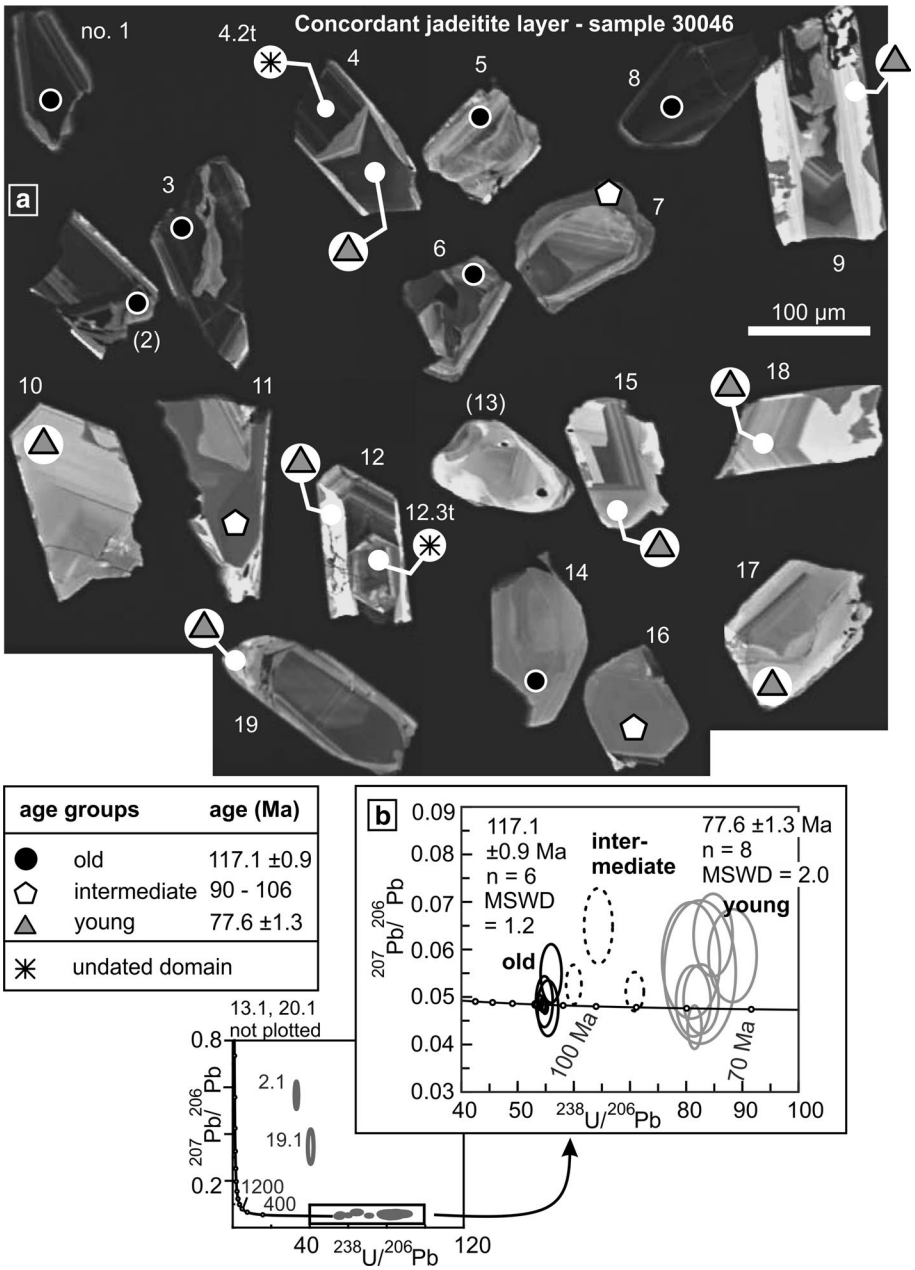

Fig. 4 Zircon morphology and results of SIMS U–Pb dating from the concordant jadeitite layer (30046). **a** CL images of the zircons showing different populations of grains of anhedral and subhedral to euhedral crystal shapes. Symbols indicate approximate position of analysis spots and the association of the particular zircon domain to a specific age group. Analyses symbolized by stars are not associated with a dated domain, but REE and trace-element data are shown in Fig. 5c–f. **b** Tera-Wasserburg diagram of U–Pb age data that allows to differentiate 3 age groups (*old, intermediate, young*). Given ages are weighted mean $^{206}Pb/^{238}U$ ages with errors representing the 95 % confidence interval; data point error ellipses are at the 1 σ level; data are uncorrected for common Pb

highest values up to 1.44. The U content of zircon is generally low but can reach up to 1000 ppm in CL-dark domains of the *old* age group. In the case of domains of the *old* and *intermediate* age groups, the incorporation of REE and P closely follows the xenotime substitution (Fig. 5f), but the substitution mechanism differs significantly from this simple exchange vector in domains of the *young* age group. The Ti content of domains of all age groups is between 1 and 12 ppm and translates to estimated equilibrium temperatures of zircon formation of ~725–800 °C for *old* and *intermediate* domains (uncorrected for pressure, $a_{TiO_2} = 0.7$, $a_{SiO_2} = 1.0$, Ferry and Watson 2007). In general, the geochemical signatures of zircon vary systematically depending on the age group, and in-group compositional variation appears highest for domains of the *young* age group.

Concordant jadeitite layer (30046): Zircon domains from different age groups occur in the same grain

As indicated in Fig. 4a, each zircon grain was dated only once, and the REE and trace-element data discussed so far apply only to these particular domains. Using the variation observed in trace-element signature as a function of age, additional trace-element analyses were collected to examine whether domains of different age groups can

Table 1 U–Pb geochronological data and apparent ages

Spot		U (ppm)	Th (ppm)	Th/U	$^{206}Pb*^{a}$	$f^{206}Pb_c^{a}$	$^{238}U/^{206}Pb^{b}$	$^{207}Pb/^{206}Pb^{b}$	$^{206}Pb/^{238}U^{c}$ (Ma)
Blueschist (30045)									
13.1	*r*	*170*	*34*	*0.21*	*2.4*	*0.2*	*61.427 (1.6)*	*0.05007 (5.6)*	*103.8 (1.7)*
12.1	r	136	23	0.18	2.0	0.7	57.172 (1.7)	0.05411 (6.0)	111.0 (2.0)
1.1	r	84	18	0.22	1.3	0.6	57.229 (2.0)	0.05326 (7.2)	111.0 (2.3)
5.1	r	201	62	0.32	3.0	0.3	57.266 (1.3)	0.05050 (4.7)	111.3 (1.5)
4.1	r	280	46	0.17	4.2	0.4	56.983 (1.3)	0.05134 (3.9)	111.7 (1.5)
3.1	r	37	7	0.19	0.6	1.0	56.104 (3.0)	0.05615 (10)	112.8 (3.5)
8.1	r	18	2	0.14	0.3	1.1	56.004 (4.2)	0.05683 (14)	112.9 (4.9)
9.1	c	172	61	0.37	2.6	0.5	56.160 (1.4)	0.05210 (4.9)	113.2 (1.6)
11.1	r	156	23	0.15	2.4	0.3	55.729 (1.5)	0.05032 (5.5)	114.4 (1.8)
10.1	r	77	10	0.14	1.2	0.7	55.362 (2.2)	0.05389 (7.9)	114.6 (2.5)
7.1	r	491	99	0.21	7.6	<0.01	55.562 (0.8)	0.04792 (2.9)	115.0 (0.9)
14.1	r	137	29	0.22	2.1	0.004	55.144 (1.6)	0.04837 (5.9)	115.8 (1.9)
6.1	c	17	2	0.09	0.3	2.1	52.387 (4.3)	0.06541 (13)	119.3 (5.3)
2.1	r	29	3	0.12	0.5	<0.01	53.304 (3.2)	0.04462 (13)	120.4 (3.9)
Concordant jadeitite layer (30046)									
20.1	r	0.2	0.01	0.05	0.002	140	80.33 (43)	1.1513 (47)	–
19.1	r	74	1.4	0.02	1.9	65	33.102 (1.9)	0.56579 (6.9)	67.0 (9.6)
12.1	r	57	1.0	0.02	0.6	1.42	88.266 (3.2)	0.05870 (11)	71.6 (2.3)
17.1	r	62	0.7	0.01	0.6	1.96	84.792 (2.7)	0.06302 (9.1)	74.1 (2.1)
9.1	r	19	0.1	0.00	0.2	0.97	82.453 (5.1)	0.05524 (18)	77.0 (4.0)
15.1	r	75	1.2	0.02	0.8	0.25	82.661 (2.5)	0.04957 (9.7)	77.3 (2.0)
10.1	r	26	0.5	0.02	0.3	1.27	80.861 (4.2)	0.05769 (14)	78.2 (3.4)
18.1	r	68	0.5	0.01	0.7	0.20	81.278 (2.5)	0.04913 (10)	78.7 (2.1)
4.1	r	411	28	0.07	4.3	<0.01	81.499 (1.0)	0.04364 (6.9)	79.0 (0.9)
7.1	*m*	*262*	*126*	*0.50*	*3.2*	*0.42*	*70.852 (1.5)*	*0.05113 (5.3)*	*90.0 (1.4)*
16.1	*m*	*55*	*54*	*1.01*	*0.7*	*2.14*	*64.371 (2.6)*	*0.06493 (8.1)*	*97.3 (2.6)*
2.1	*m*	*62*	*27*	*0.45*	*1.3*	*38*	*40.512 (2.4)*	*0.34621 (14)*	*98.6 (9.9)*
11.1	*m*	*145*	*187*	*1.33*	*2.1*	*0.57*	*59.996 (1.5)*	*0.05263 (5.2)*	*106.0 (1.6)*
14.1	m	70	29	0.43	1.1	0.84	55.958 (2.2)	0.05495 (7.4)	113.2 (2.5)
5.1	c	65	11	0.18	1.0	<0.01	55.390 (2.2)	0.04763 (8.1)	115.4 (2.6)
8.1	c	1021	255	0.26	16.0	<0.01	54.884 (0.6)	0.04793 (2.0)	116.5 (0.7)
6.1	c	103	21	0.21	1.6	0.08	54.761 (1.8)	0.04902 (7.2)	116.6 (2.1)
1.1	c	1006	248	0.25	15.9	0.00	54.523 (0.6)	0.04838 (2.1)	117.2 (0.7)
3.1	c	970	240	0.26	15.4	0.06	54.008 (0.6)	0.04883 (2.1)	118.2 (0.7)
13.1	*c*	*97*	*105*	*1.11*	*13.1*	*<0.01*	*6.370 (1.0)*	*0.06996 (1.9)*	*940.4 (9.3)*
Albite-jadeite rock (30790b)									
7.1	r	168	32	0.20	2.5	1.11	57.393 (1.3)	0.05707 (4.6)	110.1 (1.5)
5.1	r	154	25	0.17	2.3	0.39	57.530 (1.4)	0.05133 (5.0)	110.7 (1.6)
12.1	r	159	28	0.18	2.4	0.72	57.009 (1.5)	0.05399 (5.2)	111.3 (1.7)
9.1	c	142	24	0.18	2.1	0.32	57.066 (1.5)	0.05079 (5.5)	111.6 (1.7)
6.1	c	307	76	0.25	4.6	0.33	56.658 (1.1)	0.05090 (4.2)	112.4 (1.2)
11.1	c	232	34	0.15	3.5	0.15	56.480 (1.2)	0.04944 (4.3)	113.0 (1.4)
1.1	c	348	80	0.24	5.3	0.17	56.159 (1.0)	0.04962 (3.6)	113.6 (1.2)
10.1	c	94	19	0.21	1.4	0.40	55.964 (1.9)	0.05148 (6.7)	113.7 (2.3)
13.1	c	232	45	0.20	3.5	<0.01	56.127 (1.2)	0.04611 (4.5)	114.2 (1.4)
4.1	c	84	22	0.27	1.3	0.29	55.203 (2.0)	0.05067 (7.1)	115.4 (2.4)
14.1	*r*	*15*	*3*	*0.19*	*0.2*	*2.03*	*54.100 (4.7)*	*0.06446 (15)*	*115.7 (5.6)*

Table 1 continued

Spot		U (ppm)	Th (ppm)	Th/U	$^{206}Pb^{*a}$	$f^{206}Pb_c^a$	$^{238}U/^{206}Pb^b$	$^{207}Pb/^{206}Pb^b$	$^{206}Pb/^{238}U^c$ (Ma)
8.1	c	131	25	0.20	2.1	1.07	54.313 (1.6)	0.05689 (5.3)	116.4 (1.9)
3.1	r	146	18	0.13	2.3	<0.01	54.877 (1.5)	0.04670 (5.4)	116.7 (1.7)
2.1	r	244	78	0.33	3.8	0.04	54.725 (1.2)	0.04866 (4.3)	116.7 (1.4)
Jadeitite block (30825)									
10.1	*r*	*17*	*2*	*0.13*	*0.3*	*9.2*	*56.068 (4.4)*	*0.12124 (12)*	*103.5 (4.9)*
15.1	*r*	*48*	*4*	*0.08*	*0.7*	*0.8*	*57.995 (2.6)*	*0.05453 (8.3)*	*109.3 (2.9)*
12.1	*c*	*302*	*102*	*0.35*	*4.5*	*0.6*	*58.093 (1.0)*	*0.05268 (3.6)*	*109.4 (1.2)*
6.1	*r*	*287*	*74*	*0.27*	*4.3*	*0.1*	*57.930 (1.1)*	*0.04908 (4.1)*	*110.2 (1.3)*
9.1	c	289	67	0.24	4.4	0.3	56.898 (1.1)	0.05057 (4.0)	112.0 (1.3)
3.1	r	164	29	0.18	2.5	0.2	56.400 (1.4)	0.04959 (5.0)	113.1 (1.6)
16.1	r	324	64	0.20	4.9	0.2	56.384 (1.1)	0.04971 (3.9)	113.1 (1.3)
4.1	c	160	29	0.19	2.4	0.2	55.957 (1.5)	0.05010 (5.2)	113.9 (1.7)
5.1	c	422	124	0.30	6.5	0.0	55.652 (0.9)	0.04798 (3.2)	114.9 (1.1)
2.1	c	243	40	0.17	3.7	<0.01	55.627 (1.2)	0.04659 (4.2)	115.1 (1.4)
14.1	r	287	66	0.24	4.5	0.4	54.982 (1.1)	0.05129 (3.7)	115.8 (1.3)
8.1	c	314	71	0.23	4.9	0.1	55.115 (1.0)	0.04917 (3.8)	115.8 (1.2)
13.1	r	142	27	0.20	2.2	0.9	54.598 (1.5)	0.05519 (5.0)	116.0 (1.8)
11.1	r	232	68	0.30	3.7	1.1	53.756 (1.2)	0.05739 (4.1)	117.5 (1.5)
7.1	c	213	46	0.22	3.4	<0.01	54.554 (1.2)	0.04540 (4.6)	117.5 (1.5)
1.1	c	96	18	0.19	1.5	<0.01	54.111 (1.8)	0.04349 (7.0)	118.8 (2.2)

All analyses were performed on the SHRIMP-RG ion microprobe at the US Geological Survey–Stanford Microanalytical Center at Stanford University. Analytical procedure followed Williams (1998). Data reduction utilized the SQUID program of Ludwig (2001)

1.1 = grain number–spot number; c = core; r = rim

[a] Pb* denotes radiogenic Pb; Pb_c denotes common Pb; $f^{206}Pb_c = 100*(^{206}Pb_c/^{206}Pb_{total})$

[b] Calibration concentrations and isotopic compositions were based on replicate analyses of CZ3 (550 ppm U) and R33 (420 Ma, Black et al. 2004; Mattinson 2010). Reported ratios are not corrected for common Pb. Errors are reported in parentheses as percent at the 1 σ level

[c] Ages were calculated from $^{206}Pb/^{238}U$ ratios corrected for common Pb using the ^{207}Pb method (see Williams, 1998). Initial common Pb isotopic composition approximated from Stacey and Kramers (1975). Uncertainties in millions of years reported as 1 σ. Ages in italics not used in age calculation

occur together in the same zircon grain. Figures 4a and 5c–f contain additional analyses of undated zircon domains (symbolized by stars), of which two are labeled by analysis number for emphasis. In the case of grain no. 4, with a domain dated as *young*, analysis 4.2t indicates an undated domain with all the geochemical characteristics of the *old* age group. The same holds true for analysis 12.3t of grain no. 12, except for the somewhat less pronounced Ce anomaly. Both analyses show that *young*- and *old*-age-group domains do occur in a single zircon grain.

The blueschist host (30045) to the concordant jadeitite layer

Zircons separated from the blueschist host (30045) form a texturally homogeneous population of grains, which is in contrast to the heterogeneous zircon population identified in the concordant jadeitite layer. Zircon grains from the blueschist are up to 300 μm in length, sub-rounded and usually oscillatory but also patchily zoned. Some grains exhibit outer CL-bright domains separated from zircon interiors by curved resorption fronts. A Fe–Ti oxide is the only obvious primary inclusion in zircon from the blueschist; other minerals, entrapped as secondary inclusions close to edge of grains, are phengite, chlorite, titanite, omphacite and albite. Zircon grain no. 6 contains a large lawsonite inclusion (see Fig. 6a), probably of secondary origin.

U–Pb analyses of zircon from the blueschist host define a single age group with a weighted mean $^{206}Pb/^{238}U$ age of 113.6 ± 1.2 Ma (n = 13, MSWD = 1.3, see Fig. 6a) that is only slightly younger than the calculated age of the *old* zircon domains of the concordant jadeitite layer. Not considering the discordant analysis of grain no. 6, U–Pb analyses give a concordia age of 113.8 ± 1.3 Ma. The oldest $^{206}Pb/^{238}U$ dates were obtained from two CL-bright domains (119.3 ± 5.3, grain no. 6, see Fig. 6a; 120.4 ± 3.9 Ma, grain no. 2).

The chondrite-normalized REE patterns of blueschist zircon are similar to those of zircon from the *old* age group of the concordant jadeitite layer (Fig. 6b), characterized

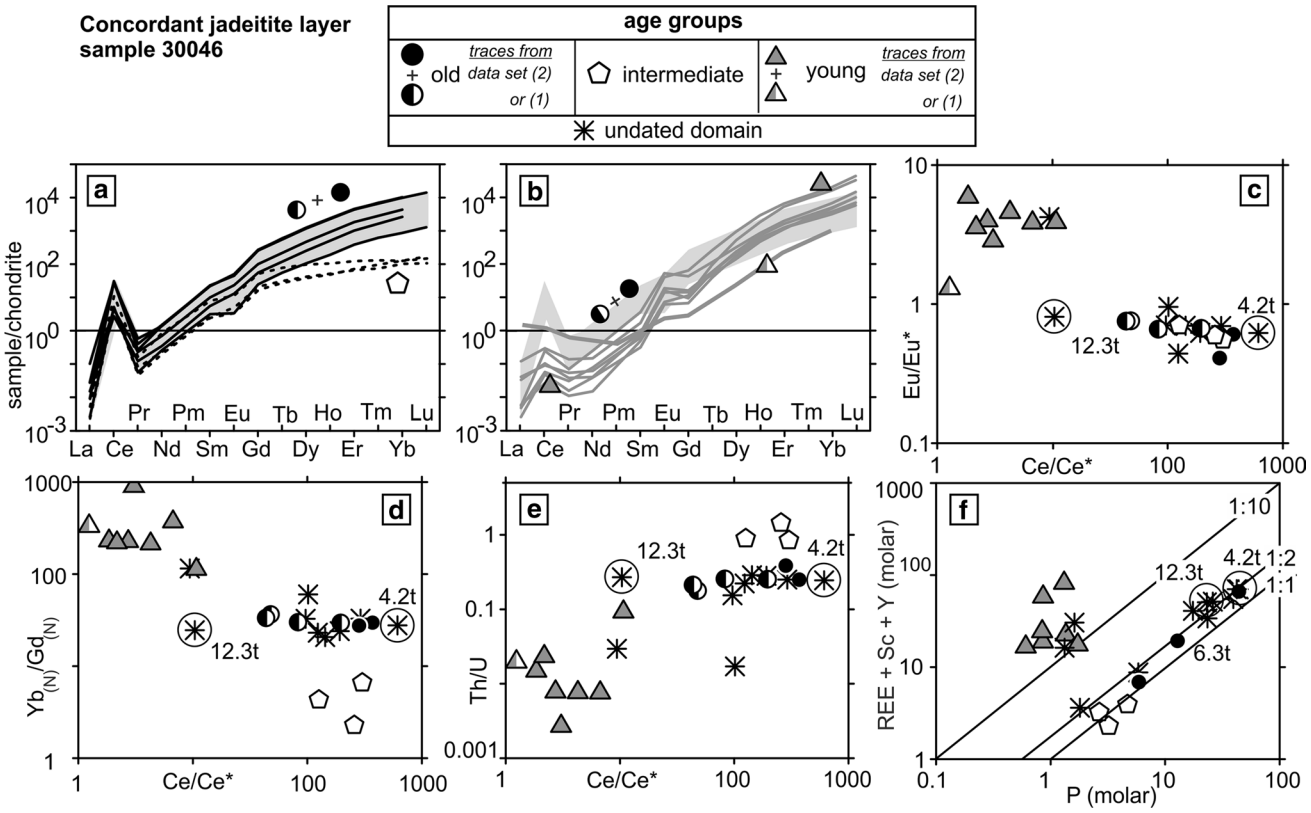

Fig. 5 REE and trace-element data of zircon from the concordant jadeitite layer (30046). **a** Chondrite-normalized REE patterns of zircon domains from the *old* and *intermediate* age groups as well as **b** *young* age group. Normalizing values are those of Anders and Grevesse (1989) multiplied by 1.36 (Korotev 1996). **c**–**e** Plots of Eu anomaly (Eu/Eu*), $Yb_{(N)}/Gd_{(N)}$ and Th/U versus Ce anomaly (Ce/Ce*) and **f** plot of Sc + Y+REE (molar) versus P (molar) illustrating possible substitution mechanisms in zircon. In all compositional plots, *old* and *young* age groups are clearly distinguishable. Analyses symbolized by stars are not associated with a dated domain, but locations of labeled analyses are shown in Fig. 4a

by pronounced positive Ce (Ce/Ce* = 18–195, $n = 10$) and negative Eu (Eu/Eu* = 0.63–0.84, $n = 11$) anomalies as well as moderately steep HREE patterns ($Yb_{(N)}/Gd_{(N)}$ = 20–43, $n = 11$). CL-bright zircon rims yield lower total REE contents; however, the overall shape of the REE patterns is similar to those of the CL-dark zircon domains (Fig. 6b). Th/U ratios of zircon from the blueschist are above 0.1 (Th/U = 0.11–0.31, $n = 11$). The substitution mechanism is close to the ideal xenotime exchange vector with lower P content for some of the rim domains (Fig. 6c); Ti contents are low (Ti = 4–16 ppm, $n = 11$) and comparable to those of zircon from the concordant jadeitite layer.

The albite-jadeite rock (30790b) and the jadeitite block (30825)

Zircons from the albite-jadeite rock (30790b) are up to 300 µm in length, sub-rounded and possess an outer, generally 5- to 20-µm-thick CL-bright rim. Zircon grains either have CL-bright cores (e.g., grain no. 8 in Fig. 6d) or do not exhibit distinct core domains (no. 1, Fig. 6d and CL images in ESM 5). Oscillatory zoning is common and most prominent in grains with CL-bright cores, but absent in overall CL-dark zircon grains. In a single zircon grain, pictured in Fig. 6d, a presumably primary mineral inclusion consisting of calcium amphibole was identified. Moreover, zircon of the albite-jadeite rock shows various secondary inclusions that are mainly composed of analcime. Zircon U–Pb analyses define a single age population with a weighted mean $^{206}Pb/^{238}U$ age of 113.4 ± 1.3 Ma ($n = 13$, MSWD = 2.0, Fig. 6d). A set of 13 analyses, some of them slightly discordant, give an almost identical concordia age of 113.8 ± 1.3 Ma. Within error, the estimated $^{206}Pb/^{238}U$ dates of core and rim domains do not differ significantly (Table 1).

Zircon grains separated from the jadeitite (30825) are sub-rounded, up to 200 µm long and faintly to well-pronounced oscillatory (Fig. 6d) or unevenly zoned. Some grains possess irregularly shaped CL-bright rim domains. Primary mineral inclusions are absent in zircon from this sample. U–Pb analyses give a weighted mean $^{206}Pb/^{238}U$ age of 115.0 ± 1.2 Ma ($n = 12$, MSWD = 1.7, Fig. 6d);

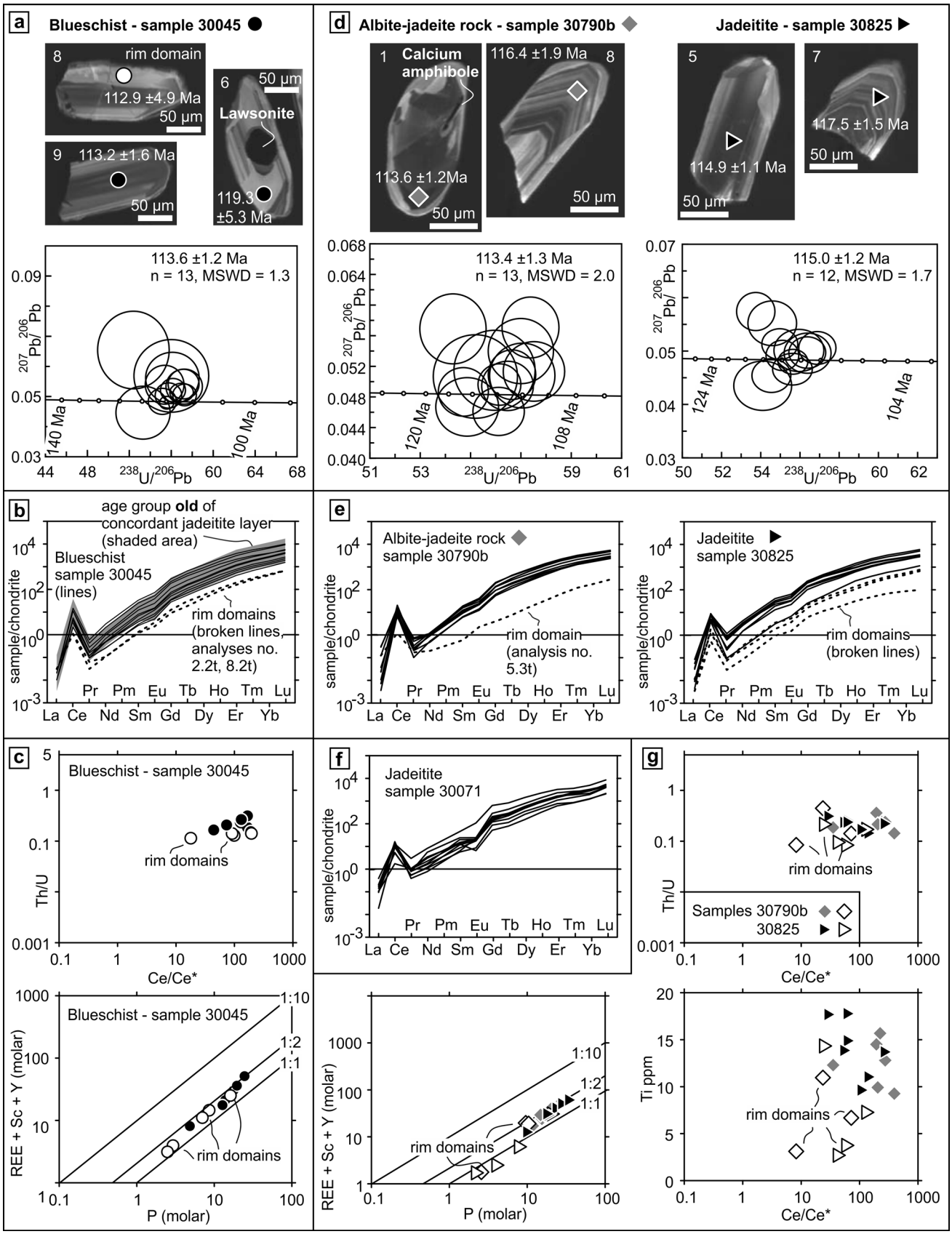
a
Blueschist - sample 30045
8
rim domain
112.9 ±4.9 Ma
50 µm
9
113.2 ±1.6 Ma
50 µm
6
50 µm
Lawsonite
119.3 ±5.3 Ma
113.6 ±1.2 Ma
n = 13, MSWD = 1.3
140 Ma
100 Ma
d
Albite-jadeite rock - sample 30790b
Jadeitite - sample 30825
1
Calcium amphibole
113.6 ±1.2Ma
50 µm
116.4 ±1.9 Ma
8
50 µm
113.4 ±1.3 Ma
n = 13, MSWD = 2.0
120 Ma
108 Ma
5
114.9 ±1.1 Ma
50 µm
7
117.5 ±1.5 Ma
50 µm
115.0 ±1.2 Ma
n = 12, MSWD = 1.7
124 Ma
104 Ma
207Pb/206Pb
238U/206Pb
b
age group old of concordant jadeitite layer (shaded area)
Blueschist sample 30045 (lines)
rim domains (broken lines, analyses no. 2.2t, 8.2t)
sample/chondrite
e
Albite-jadeite rock sample 30790b
rim domain (analysis no. 5.3t)
Jadeitite sample 30825
rim domains (broken lines)
La Ce Nd Sm Gd Dy Er Yb
Pr Pm Eu Tb Ho Tm Lu
c
Blueschist - sample 30045
rim domains
Th/U
Ce/Ce*
REE + Sc + Y (molar)
1:10
1:2
1:1
P (molar)
f
Jadeitite sample 30071
g
Samples 30790b
30825
Ti ppm

◀**Fig. 6** Zircon morphology, results of SIMS U–Pb dating as well as REE and trace-element data of zircon from the blueschist (30045), the albite-jadeite rock (30790b), the jadeitite block (30825) and REE patterns of zircon from the phengite-rich jadeitite (30071). **a**, **d** CL images of zircon and Tera-Wasserburg diagrams. Quoted ages are weighted mean $^{206}Pb/^{238}U$ ages with errors representing the 95 % confidence interval; data point error ellipses are at the 1 σ level; data are uncorrected for common Pb. **b**, **e**, **f** Chondrite-normalized REE patterns of zircon. The overall shapes of patterns of CL-bright rim domains are similar to those of core domains, but REE are slightly depleted relative to core domains. Normalizing values are those of Anders and Grevesse (1989) multiplied by 1.36 (Korotev 1996). **c**, **g** Th/U, $Yb_{(N)}/Gd_{(N)}$ and Ti versus Ce anomaly (Ce/Ce*) plots as well as Sc + Y+REE (molar) versus P (molar) diagrams. CL-bright rim domains usually yield slightly lower Th/U ratios and lower molar amounts of P and Ti

neglecting the slightly discordant analyses of grains no. 11 and 13, the jadeitite (30825) yields a concordia age of 114.9 ± 0.4 Ma.

The chondrite-normalized REE patterns of zircon from samples 30790b and 30825 (Fig. 6e) show pronounced positive Ce (Ce/Ce*; 30790b: 8–392, $n = 9$; 30852: 24–262, n = 11) and negative Eu (Eu/Eu*; 30790b: 0.59–0.72, anal. 5.3t = 1.47, $n = 9$; 30825: 0.58–0.76, $n = 11$) anomalies, as well as moderately steep HREE patterns ($Yb_{(N)}/Gd_{(N)}$; 30790b: 19–45, $n = 9$; 30825: 12–33, $n = 11$, Fig. 6e). Except for some of the CL-bright rim domains, zircon of both samples possesses Th/U ratios greater than 0.10 (Th/U; 30790b: 0.08–0.44, $n = 9$; 30825: 0.08–0.31, $n = 11$; Fig. 6g); the U content is never higher than 450 ppm and lowest in zircon rims. The mechanism of REE incorporation is close to the ideal xenotime substitution; for both samples, Ti (30790b: 3–16 ppm, $n = 9$; 30825: 3–18, $n = 11$, Fig. 6g) and P contents are lowest in CL-bright rim domains. Estimated equilibrium temperatures of zircon formation are in the range of 675–830 and 660–840 °C (uncorrected for pressure, $a_{TiO_2} = 0.7$, $a_{SiO_2} = 1.0$, Ferry and Watson 2007) for the albite-jadeite rock (30790b) and jadeitite (30825), respectively. In summary, the geochemical signatures of zircon from the albite-jadeite rock (30790b) and the jadeitite (30825) are similar to those of zircon from the *old* age group of the concordant jadeitite as well as to those of zircon from the blueschist sample.

The phengite-rich jadeitite (30071)

Textural features and geochronological data of zircon from the phengite-rich jadeitite (30071) are given in Schertl et al. (2012) and can be summarized as follows: Zircon grains are usually euhedral and oscillatory zoned; some of the grains possess CL-bright, faintly oscillatory zoned rim domains. Core domains yield a concordia-intercept age of 114.9 ± 2.9 Ma ($n = 5$); rim domains are slightly younger and yield a poorly defined intercept age of 93.3 ± 6.9 Ma ($n = 4$). Th/U ratios of the core domains scatter between 0.15 and 0.32 ($n = 5$) and between 0.09 and 0.49 ($n = 4$) for the CL-bright rims (Schertl et al. 2012).

Figure 6f shows the REE patterns of zircon from the phengite-rich jadeitite (30071). Chondrite-normalized REE patterns possess a positive Ce anomaly (5–84, $n = 10$), a negative Eu anomaly (0.26–0.64, $n = 10$) and moderately steep HREE slope (8–24, $n = 10$). There is no discernible difference between core and rim domains. The moderately high Th/U ratios in conjunction with the shape of the REE patterns suggest a strong geochemical similarity to zircon from the albite-jadeite rock (30790b), the jadeitite (30825) and the *old* zircon domains of the concordant jadeitite layer (30046) as well its blueschist host (30045).

Oxygen isotope analysis of zircon

In order to further characterize the geochemical environment during zircon growth or recrystallization (Valley 2003; Valley et al. 2005), oxygen isotope analyses of zircon were carried out and the respective data are given in Table 2 as well as ESM 4. Figure 7a shows the individual $\delta^{18}O(Zrn)$ analyses of the dated zircon domains from the concordant jadeitite layer. Individual domains of zircons were analyzed up to seven times, and the average values of domains were used to calculate a mean for the specific age groups. On average, oxygen isotope ratios of *old* domains (mean of age group, 5.36 ± 0.39 ‰ VSMOW, 2 SD, number of domains $n = 6$) are considerably lower than ratios of the *young* age group (6.33 ± 0.77 ‰ VSMOW, 2 SD, $n = 8$), and, in general, oxygen isotope ratios of the *young* age group are more variable and diverge more strongly from the mean of the group than values of the *old* age group do. Oxygen isotope ratios of individual *intermediate* domains are highly heterogeneous (2SD = 0.56–0.92 ‰ VSMOW; in-grain variation), and averages of each *intermediate* domain sum up to an age group average (5.72 ± 0.20 ‰ VSMOW, 2 SD, $n = 3$) that is indistinguishable from those of either the *old* or *young* age groups. The oxygen isotope ratios of undated zircon domains that correspond to trace-element analyses 4.2t and 12.3t (see Fig. 7a and compare Figs. 4a and 5c–f) are lower than the ratios of the corresponding *young* zircon domains, therefore strengthening the interpretation that they indeed belong to the *old* zircon domains of the jadeitite layer.

A representative $\delta^{18}O(Zrn)$ value of blueschist zircon was obtained by averaging oxygen isotope ratios of individual grains and subsequently aggregating these grain means to a single isotope ratio. This averaging approach is reasonable, because CL-bright zircon rims are not consistently enriched or depleted in ^{18}O relative to CL-dark domains (see ESM 4). The determined value of zircon from the blueschist host (5.65 ± 0.58 ‰ VSMOW, 2 SD, $n = 14$,

Table 2 Compilation of $\delta^{18}O$(Zrn) values (‰VSMOW) of zircon grains/domains of the concordant jadeitite layer (30046, only dated domains), the blueschist (30045), the albite-jadeite rock (30790b) and the jadeitite block (30825)

Grain No.	Date Ma, 1 SD	Age group	$\delta^{18}O$ mean	1 SD	$\delta^{18}O$ min	$\delta^{18}O$ max	N
Concordant jadeitite layer (30046)							
1	117.2 ± 0.7	Old	5.24	0.40	4.91	5.68	3
3	118.2 ± 0.7	Old	5.34	0.23	5.08	5.52	3
4	79 ± 0.9	Young	6.16	0.14	6.06	6.26	2
5	115.4 ± 2.6	Old	5.63				1
6	116.6 ± 2.1	Old	5.37	0.09	5.27	5.45	3
7	90 ± 1.4	Interm.	5.82	0.46	5.19	6.61	7
8	116.5 ± 0.7	Old	5.08	0.08	4.98	5.13	3
9	77 ± 4.0	Young	6.61	0.69	5.89	7.20	4
10	78.2 ± 3.4	Young	6.46	0.11	6.39	6.54	2
11	106 ± 1.6	Interm.	5.62	0.28	5.26	5.89	6
12	71.6 ± 2.3	Young	5.86				1
14	113.2 ± 2.5	Old	5.51	0.45	5.19	5.83	2
15	77.3 ± 2.0	Young	6.58	0.25	6.40	6.76	2
16	97.3 ± 2.6	Interm.	5.72	0.41	5.02	6.36	7
17	74.1 ± 2.1	Young	6.89	0.35	6.53	7.23	3
18	78.7 ± 2.1	Young	5.77	0.20	5.62	6.12	5
19	67 ± 9.6	Young	6.29				1
Mean of age groups							
		Young	6.33	0.38	5.77	6.89	8
		Interm.	5.72	0.10	5.62	5.82	3
		Old	5.36	0.19	5.08	5.63	6
Blueschist (30045)							
1			5.28	0.19	5.07	5.40	3
2			5.16	0.04	5.12	5.21	3
3			5.77	0.68	4.90	6.52	4
4			5.55	0.24	5.24	5.80	4
5			5.79	0.18	5.66	5.92	2
6			6.05	0.49	5.61	6.75	4
7			5.45	0.62	4.67	6.09	4
8			5.80	0.51	5.27	6.46	4
9			6.01	0.39	5.74	6.45	3
10			5.96	0.42	5.56	6.40	3
11			5.23	0.08	5.17	5.29	2
12			5.51	0.52	5.04	6.32	5
13			5.82	0.52	5.21	6.49	7
14			5.72	0.41	5.43	6.01	2
Sample mean			5.65	0.29	5.16	6.05	14
Albite-jadeite rock (30790b)							
1			4.91	0.37	4.57	5.34	4
2			5.07	0.32	4.69	5.28	3
3			5.08	0.33	4.74	5.39	3
4			5.15	0.17	5.03	5.26	2
5			4.43	0.02	4.42	4.44	2
6			4.20				
7			4.33	0.16	4.21	4.44	2
8			4.71	0.51	4.35	5.07	2
9			4.81	0.14	4.66	4.94	3
10			4.44				
11			3.92				

Table 2 continued

Grain No.	Date Ma, 1 SD	Age group	δ^{18}O mean	1 SD	δ^{18}O min	δ^{18}O max	N
12			4.27	0.24	4.10	4.43	2
13			4.43				
14			4.80	0.38	4.53	5.08	2
Sample mean			4.61	0.38	3.92	5.15	14
Jadeitite block (30825)							
1			5.12				
2			5.12				
3			5.05				
4			4.63				
5			5.00	0.33	4.76	5.23	2
6			5.59				
7			4.82				
8			5.38	0.17	5.19	5.53	3
9			5.16	0.31	4.95	5.38	2
11			4.88	0.44	4.39	5.26	3
13			5.47				
14			5.01				
15			5.52	0.30	5.31	5.73	2
16			5.13				
Sample mean			5.13	0.28	4.63	5.59	14

Fig. 7b) is similar within error to the oxygen isotope ratio of the *old* zircon domains from the jadeitite layer (30046, Fig. 7a, shaded area).

There is no resolvable difference in the δ^{18}O(Zrn) ratios of the CL-bright and CL-dark domains of zircon from the albite-jadeite rock (30790b) and the jadeitite (30825), although, especially for the albite-jadeite rock, the precision of analyses may have obscured in-grain variations that are smaller than 1 ‰ (see Fig. 3). Zircon from the albite-jadeite rock (30790b) possesses the lowest δ^{18}O(Zrn) values (4.61 ± 0.76 ‰ VSMOW, 2 SD, $n = 14$, Fig. 7c); zircon from the jadeitite (30825) shows an average oxygen isotope ratio (5.13 ± 0.56 ‰ VSMOW, 2 SD, $n = 14$, Fig. 7d) that is similar within error to the ratio of zircon from the blueschist and the *old* age group from the jadeitite layer.

Discussion

Zircon in P- and R-type jadeitites

On the basis of the mode of formation, jadeitites are classified into P-type, if crystallized directly from an aqueous fluid, or R-type, if they are considered to represent a product of a metasomatic replacement process. Zircon is a common accessory mineral in jadeitites worldwide (e.g., Harlow et al. 2015), and, in principle, may (1) be inherited from an igneous protolith (implying R-type process of jadeitite genesis), (2) have grown simultaneously with the jadeite from an aqueous fluid or hydrous melt (both P-type and R-type formation of jadeitites possible) or (3) represent an igneous xenocryst transported by the jadeitite-forming fluid/melt to the site of jadeitite genesis (P-type formation). Hereafter, the term "igneous" will be used for zircon that grew in a melt phase; zircon that has been precipitated from an aqueous fluid in a metamorphic environment will be called "metamorphic." Several studies have confirmed that igneous and metamorphic zircon may significantly differ from each other in terms of their REE and trace-element (Schaltegger 1999; Rubatto 2002; Hoskin and Schaltegger 2003; Hoskin 2005; Rubatto and Hermann 2007; Geisler et al. 2007; McClelland et al. 2009; Mattinson et al. 2009) as well as oxygen isotope signatures (Valley et al. 2003; Page et al. 2007b; Fu et al. 2010, 2013; Grimes et al. 2013; Rubatto and Angiboust 2015). To be conclusive, zircon studies on jadeitites need to be capable of reliably differentiating between zircon crystallized in a high-temperature low-pressure igneous environment and zircon grown under high pressures and relatively low temperatures during subduction-zone metamorphism.

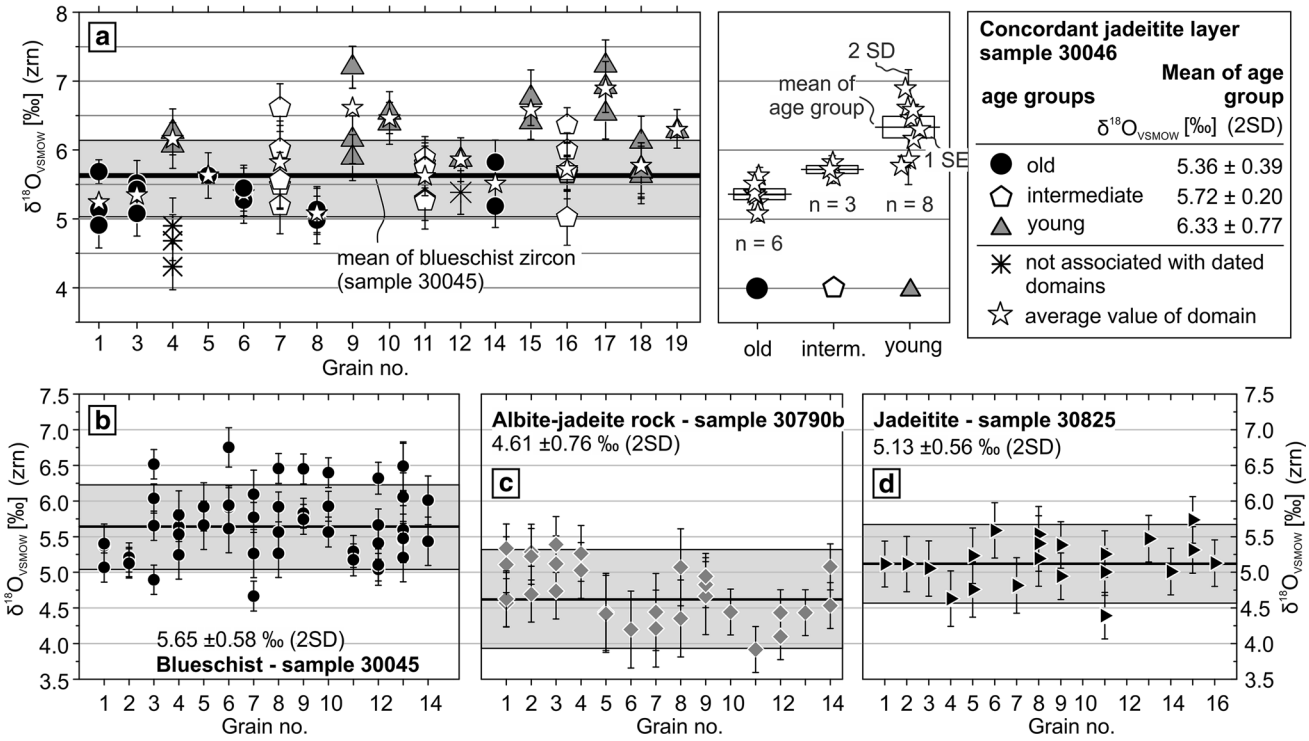

Fig. 7 Results of oxygen isotope analysis of zircon ($\delta^{18}O_{VSMOW}$) for **a** the jadeitite layer (30046), **b** the blueschist host (30045), **c** the albite-jadeite rock (30790b) and **d** the jadeitite (30825). *Error bars* (±2 SD) represent the estimated analytical error as defined by repeated analyses of zircon oxygen isotope standard KIM-5 (see section on Analytical methods). Oxygen isotope ratios of *old* zircon domains are consistently lower than those of *young* domains; *intermediate* domains are indistinguishable from *old* zircon domains. Location of analyses that are symbolized by stars (see grains 4 and 12) corresponds to location of respective REE and trace-element analyses 4.2t and 12.3t *highlighted* in Figs. 4a and 5c–e

Distinguishing igneous from metamorphic zircon

So far, no generally applicable geochemical discriminants have been found that reliably differentiate between igneous and metamorphic zircon. Hoskin (2005) used discrimination diagrams for magmatic and hydrothermal zircon based on the extent of the Ce anomaly, La concentrations and the slope of the light REE (LREE). However, as discussed by Fu et al. (2009), these discrimination plots seem not to be universally applicable to hydrothermal zircon. In addition, the Th/U ratio has commonly been considered as a strong indicator of whether zircon is igneous or metamorphic, and low ratios (Th/U < 0.1) are attributed to metamorphic zircon (Rubatto 2002; Rubatto and Hermann 2007). However, Th/U ratios of metamorphic zircon have been found to be very variable and often above the threshold value (Harley et al. 2007, and references therein). As highlighted by Yui et al. (2013), individual zircon domains can show typical igneous as well as metamorphic geochemical and isotopic signatures due to incomplete recrystallization of igneous zircon, which in turn is caused by different resetting rates of the various trace-element and U–Pb isotope systems in zircon. Therefore, it is important to evaluate the zircon analyses on a sample-by-sample basis and to combine geochemical tools with accompanying methods such as morphological inspection of zircon and mineral inclusion studies (Rubatto and Hermann 2007). In addition, the oxygen isotope composition of zircon can help to distinguish igneous from metamorphic zircon (Fu et al. 2010, 2013; Rubatto and Angiboust 2015) and serve as an indicator for zircon growth during high-pressure metamorphism (Grimes et al. 2013).

In order to determine whether the zircons investigated here are of igneous or metamorphic origin, the geochemical and isotopic signatures of zircon from the jadeite rocks as well as the blueschist are compared to those of exemplary igneous zircon, obtained from oceanic plagiogranites and gabbros of the oceanic lithosphere (Fig. 8a). Zircon from modern oceanic lithosphere shows REE patterns with well-developed positive Ce anomalies, pronounced negative Eu anomalies and moderately steep HREE patterns (shaded areas in Fig. 8a–e) (Grimes et al. 2007, 2009; Cavosie et al. 2009). The oxygen isotope compositions of zircon from modern oceanic lithosphere fall within a narrow range of 5.2 ± 0.5 ‰ (VSMOW, 2 SD; Grimes et al. 2011) that matches the $\delta^{18}O$(Zrn) ratios of zircon crystallized

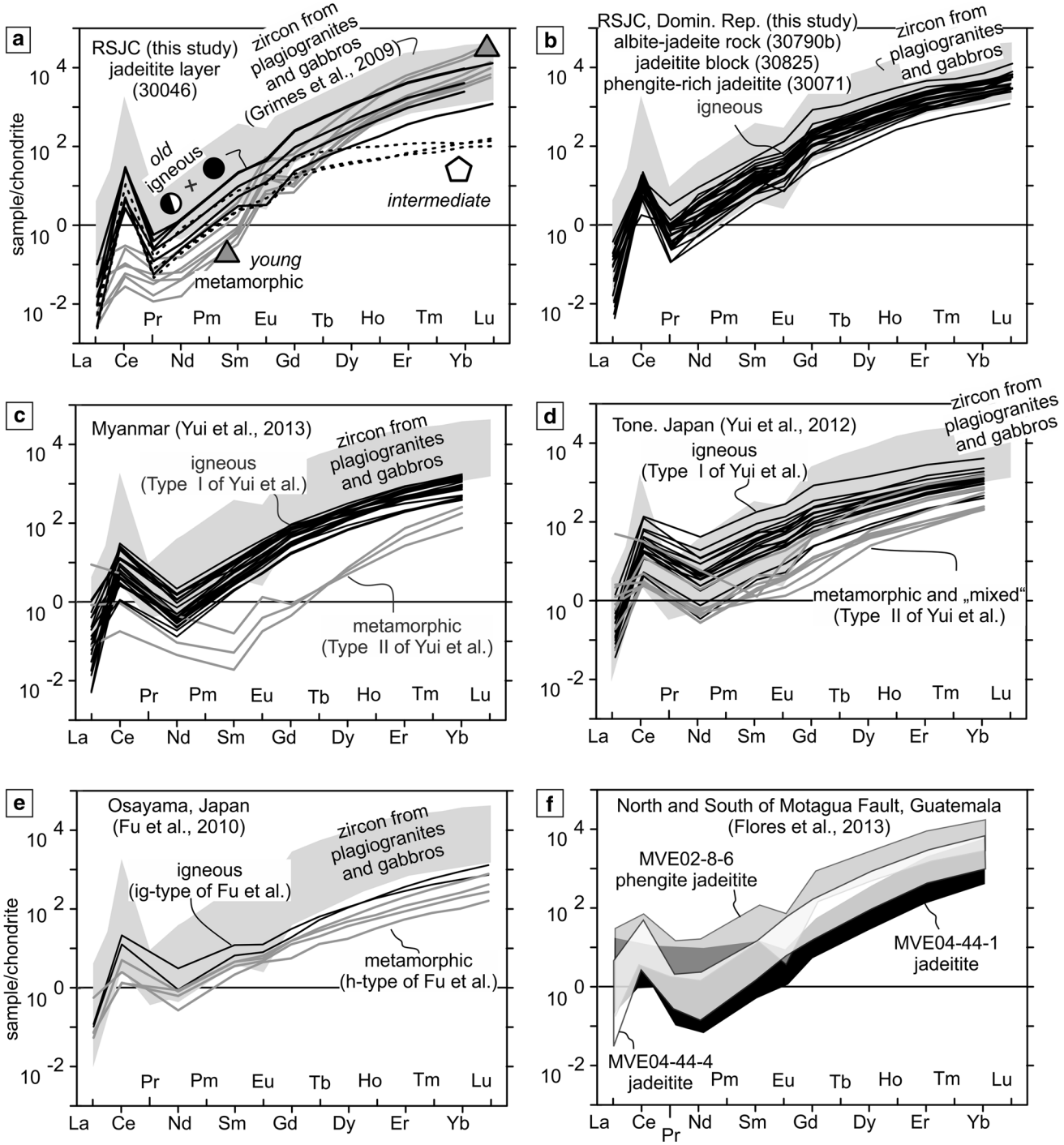

Fig. 8 Chondrite-normalized REE patterns of zircon from jadeite rocks of the RSJC **a**, **b** as well as other jadeitite localities **a**–**f** in comparison with REE patterns of zircon from the igneous oceanic lithosphere (*shaded fields* in **a**–**e**, oceanic plagiogranites and gabbros; Grimes et al. 2009). REE patterns of zircon from **a** the *old* age group (30046, jadeitite layer) and **b** zircon from the albite-jadeite rock (30790b), the jadeitite block (30825), as well as the phengite-rich jadeitite (30071) are indistinguishable from REE patterns of igneous zircon from oceanic plagiogranites. REE patterns of zircon from **c** the Myanmar (Yui et al. 2013) and **d** the Tone jadeitites (Yui et al. 2012) show igneous domains that possess similar pattern such as those of zircon from oceanic plagiogranites. Metamorphic zircons from the Myanmar jadeitite possess distinct patterns (e.g., positive Eu anomaly) similar to those of age group *young* domains from the jadeitite layer (30046). **e** Igneous and metamorphic domains of zircon from the Osayama jadeitite (Fu et al. 2010) are indistinguishable in terms of REE patterns and are depleted in HREE relative to oceanic plagiogranites. **f** REE patterns of zircon from North and South of Motagua Fault Zone (Flores et al. 2013) are highly variable; sample MVE02-8-6 shows REE patterns similar to those of igneous zircon (only patterns considered where analyses spot smaller than zircon grain; Flores et al. 2013)

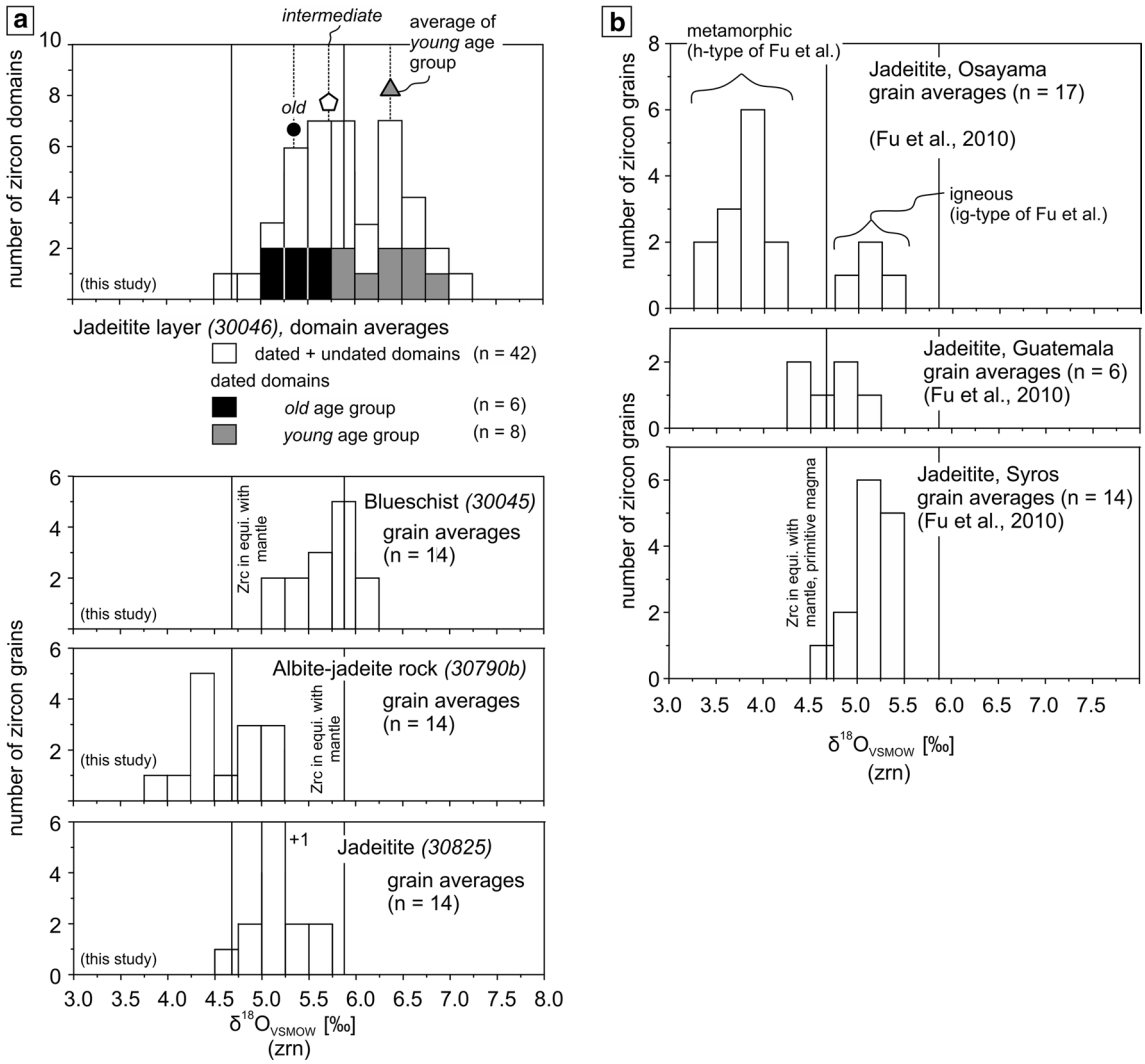

Fig. 9 Histograms showing $\delta^{18}O$(Zrn) values of zircon from **a** jadeite rocks and blueschist from the RSJC and **b** jadeitites from three other localities (Fu et al. 2010). *Old* and *intermediate* zircon domains from the jadeitite layer (30046), zircon from the blueschist (30045), as well as the jadeitite block (30825) yield mean $\delta^{18}O$(Zrn) values similar to those of zircon formed in equilibrium with the mantle (5.3 ± 0.6 ‰, VSMOW, 2 SD; Valley et al. 2005). Primitive mantle-like $\delta^{18}O$(Zrn) values are typical for igneous zircon from oceanic lithosphere (Grimes et al. 2011). The albite-jadeite rock yields slightly lower, but within error identical values. **b** $\delta^{18}O$(Zrn) values of igneous zircon from Osayama jadeitite are identical to mantle-like values; metamorphic zircon possesses lower values. Zircon from Guatemala (Fu et al. 2010) and Syros, Greece (Fu et al. 2010), shows mainly mantle-like $\delta^{18}O$(Zrn) ratios

in equilibrium with primitive mantle compositions (see Fig. 9a, 5.3 ± 0.6 ‰, VSMOW, 2 SD; Valley et al. 1998, 2005; Valley 2003; Page et al. 2007a). Neither the REE patterns and trace-element compositions nor the oxygen isotope signatures of zircon from oceanic plagiogranites and gabbros differ significantly from each other (Grimes et al. 2009, 2011).

Igneous and metamorphic zircon in jadeite rocks of the Dominican Republic

Zircon of the *old* age group from the jadeitite layer (30046) possesses REE patterns that are indistinguishable from those of igneous zircon from oceanic plagiogranites (Fig. 8a) in terms of Ce and Eu anomalies as well as the slope of the HREE. In addition, the Th/U ratio of these domains is consistently above 0.1, typical for zircon from oceanic plagiogranites (normal magmatic zircon; Grimes et al. 2009); the mean $\delta^{18}O$(Zrn) ratio of this age group is within error similar to ratios obtained for zircon of oceanic plagiogranites as well (zircon in equilibrium with mantle composition, Fig. 9a). Therefore, we interpret the *old* zircon domains from the jadeitite layer (30046) to be igneous in origin and to have been inherited from an igneous jadeitite protolith.

The blueschist zircon (30045) as well as zircon from the albite-jadeite rock (30790b) and the jadeitite block

(30825) possess REE patterns (Fig. 8b), Th/U ratios and, except for the albite-jadeite rock, $\delta^{18}O$(Zrn) values (Fig. 9a) which are similar to those of the *old* age group (30046) and zircon from oceanic lithosphere. Zircon from the albite-jadeite rock yields slightly lower, but within error identical $\delta^{18}O$(Zrn) ratios. We conclude, therefore, that zircon from these samples does not yield any conspicuous geochemical signatures, nor do zircon grains possess any primary jadeite inclusions that would substantiate the interpretation that zircon might have precipitated from an aqueous fluid simultaneously with formation of the jadeite. The CL-bright rim domains of some of the zircon show depleted REE and trace elements relative to core domains, which is considered typical for altered (or annealed) igneous zircon domains (Hoskin and Black 2000; Geisler et al. 2007).

In contrast, zircon domains of the *young* age group of the jadeitite layer (30046) are very distinct from zircon of modern oceanic lithosphere. *Young* domains exhibit less pronounced positive Ce anomalies, positive instead of negative Eu anomalies, steeper HREE patterns (Fig. 8a), lower Th/U ratios (<0.1) and a REE incorporation mechanism that does not follow the xenotime substitution. In addition, the mean $\delta^{18}O$(Zrn) ratio of this age group is considerably higher than values typical for zircon from igneous oceanic crust (Fig. 9a). *Young* zircon domains are likely metamorphic in origin and might have either precipitated as entire grains from a hydrothermal fluid (e.g., grain no. 18, see Fig. 4a) or have formed by a coupled dissolution–reprecipitation process affecting the outer domains of parent igneous grains (e.g., grains no. 4, 12, see Fig. 4a) (Geisler et al. 2007). However, the absence of jadeite inclusions in these domains does not permit a direct link between the growth of the *young* zircon domains and the actual formation of jadeitite.

The *intermediate* domains differ from *old*-age-group domains (30046) in terms of their flatter HREE patterns and higher Th/U ratios, whereas the extent of Ce and Eu anomalies as well as the $\delta^{18}O$(Zrn) ratios is similar for both age groups. *Intermediate* domains likely belong to altered igneous zircons that could have lost HREE due to subsolidus recrystallization (Hoskin and Black 2000; Rubatto 2002) or by exchange with a fluid/melt with lowered HREE concentrations (e.g., due to garnet growth prior or concurrent with zircon exchange; Rubatto and Hermann 2007).

The single Proterozoic grain observed within the zircon population of the jadeitite layer (30046) could represent recycled material that was incorporated into the source of the protolith-forming melt. Zircon grains that are older than the protolith age of the metamorphic rock have also been described from an eclogite within the Monviso Ophiolite (Rubatto and Hermann 2003) and a gabbro from the Vourinos Ophiolite Complex (Liati et al. 2004).

Igneous zircon crystallized from anatectic (subduction-related) or mantle-derived melts?

Overall, the age group of *old* zircon domains from the concordant jadeitite layer and zircon from the albite-jadeite rock (30790b), the jadeitite (30825) and the phengite-rich jadeitite (30071) is indistinguishable from igneous zircon of oceanic crust and there is no evidence that would point to a metamorphic origin of the investigated zircon (domains). Consequently, it is unlikely that the above-mentioned zircons precipitated from an aqueous fluid simultaneously with jadeite at high pressures and relatively low temperatures (<500 °C). Some of the geochemical signatures, such as the negative Eu anomaly, may be found in zircon that formed in the presence of a melt at metamorphic conditions (Rubatto 2002), which raises the question whether these igneous zircons could have crystallized from anatectic melts rather than from mantle-derived melts formed at a mid-ocean ridge.

As Koepke et al. (2007) summarize, oceanic plagiogranites—potential protoliths of jadeite rocks—are commonly regarded either as products of highly differentiated MORB melts (e.g., Coleman 1977; Floyd et al. 1998) or represent partial lower crustal melts of gabbroic material (Koepke et al. 2004, 2007). Furthermore, partial melting of amphibolites during hot subduction accompanied by small-scale melt migration (e.g., Lázaro et al. 2009) or emplacement of partial slab melts into the overriding plate during incipient subduction (Goodenough et al. 2014) can form felsic lithologies within oceanic lithosphere. Thus, the general term "oceanic plagiogranites" denotes highly variable leucocratic rocks in modern and ancient oceanic lithosphere and implicates a wide range of geological settings in which these potential protoliths of jadeite rocks might have formed. Grimes et al. (2011, 2013) measured oxygen isotope ratios in igneous zircons from plagiogranite and found values that are generally in high-temperature equilibrium with pristine MORB.

Based on trace-element geochemistry of zircon, Grimes et al. (2015) recently proposed a series of "comparative discrimination diagrams," helpful for deducing the geotectonic setting of plagiogranite formation. Extending the work of Grimes et al. (2007), the authors show that igneous zircon from different geotectonic settings (mid-ocean ridge, magmatic arc, ocean island setting) differs with respect to trace-element contents and ratios such as U/Yb, Nb/Yb and Sc/Yb. Consequently, zircon from mantle-derived melts (MOR) can be distinguished from zircon crystallized in subduction-related melts (magmatic arc) among an otherwise geochemically homogeneous zircon population (e.g., similar extent of Eu and Ce anomalies, general shape of REE patterns, Th/U ratios). In Fig. 10a and b, two of the proposed discrimination diagrams are applied to

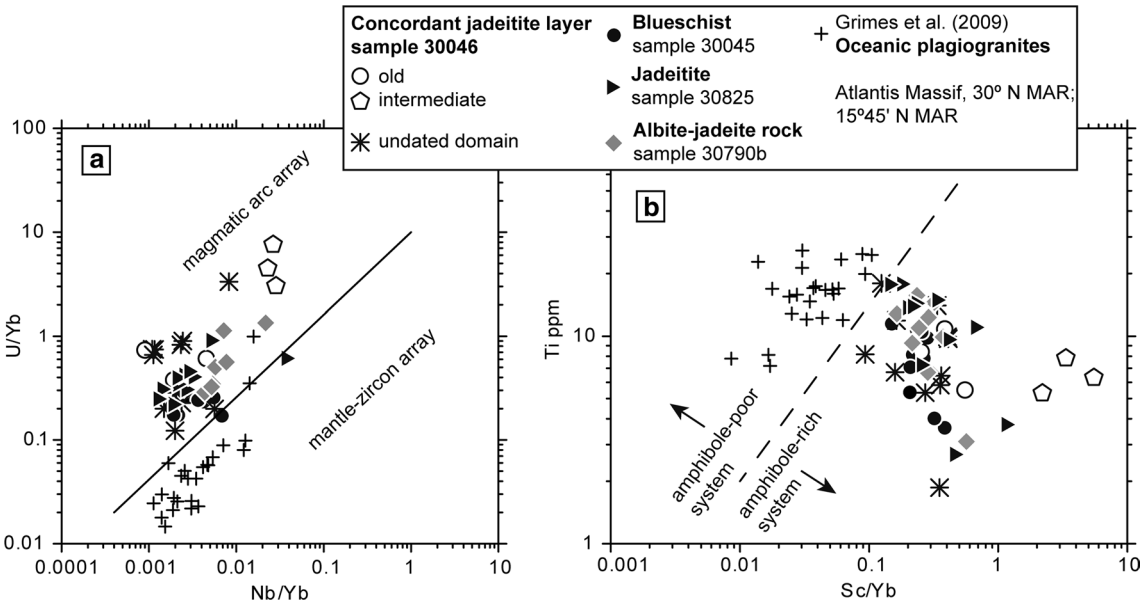

Fig. 10 Discrimination diagrams developed by Grimes et al. (2015) for determining tectono-magmatic provenance of igneous zircon. Application of the **a** U/Yb–Nb/Yb and **b** Ti–Sc/Yb diagrams to igneous zircon from this study. Most of the zircon from jadeite rocks and blueschist show affinity to the magmatic arc array, while zircon from oceanic plagiogranites, investigated by Grimes et al. (2009), possesses trace-element ratios and Ti contents indicative for mantle-derived zircon

zircon from the concordant jadeitite layer (30046, excluding *young* zircon domains), the blueschist (30045), the albite-jadeite rock (30790b) and the jadeitite (30825) as well as to plagiogranite zircon from in situ oceanic crust close to the Mid-Atlantic Ridge (Grimes et al. 2009). Virtually all zircons from the samples investigated here show a clear magmatic arc affinity using the U/Yb and Sc/Yb proxies (amphibole-rich system), whereas the limited data set of zircon from oceanic plagiogranites indicates mantle-zircon affinity.

According to Grimes et al. (2015), abnormally high U/Yb values in zircon crystallized in mantle-derived melts may be caused by an extreme degree of differentiation. However, zircon from jadeite rocks and blueschist yields Hf contents below 15,000 ppm (see ESM 2), thus not indicating highly evolved melts. Furthermore, the presence or absence of amphibole potentially controls trace-element contents of zircon in combination with the degree of differentiation and the presence of accessory phases (Grimes et al. 2015). Hydrous partial melting of a gabbroic protolith, as proposed by Koepke et al. (2004, 2007) for plagiogranite petrogenesis, involves amphibole as one of the reaction products, and zircon that grew in such a melt could possess substantially higher U/Yb values, thus indicating an arc-like affinity (Grimes et al. 2015). Consequently, zircon in the jadeite rocks studied here is likely inherited from plagiogranite protoliths that crystallized from partial anatectic melts rather than mantle-derived melts, but the question whether the plagiogranites formed close to a mid-ocean ridge or in the vicinity of a subduction zone cannot be answered conclusively.

Formation of the protoliths of jadeite rocks

Hertwig (2014) compared the major element, minor element and REE contents of the various jadeite-bearing rocks of the RSJC with available geochemical data on oceanic plagiogranites. He found that some types of jadeite rocks can exhibit an essentially isochemical correspondence with sampled and analyzed igneous plagiogranites. For others, primarily a desilication and metasomatic addition of CaO and/or Na_2O is required. The geochemical correspondence is so robust that plagiogranites as a group can be viewed as logical potential protoliths. We consider it unlikely that in the RSJC serpentinite mélange the majority of the jadeite rocks can be considered to be P-type with exotic entrained igneous zircon (cf., Meng et al. 2016). With this assumption, potential jadeitite protoliths must be sought in the Great Arc subduction-zone system.

Geochemically appropriate rocks exist in the northern RSJC, but available geochronological data suggest that protolith analogues of the jadeite rocks investigated here are currently not exposed in the northern RSJC (crystallization age of a leucotonalite intrusion: 71.3 ± 0.7 Ma, Escuder-Viruete et al. 2013a; lawsonite-bearing metatrondhjemite, protolith age: 94.7 ± 3.1 Ma, Krebs 2008, see section on geological setting). However, trondhjemitic to tonalitic rocks that possess crystallization ages

in good agreement with ages of the igneous zircon of this study (~113–117 Ma) are known from the Sierra del Convento (112.8 ± 1.1 Ma, Lázaro et al. 2009) and La Corea (~105–110 Ma, Blanco-Quintero et al. 2011a) serpentinite mélanges in eastern Cuba. In these localities, tonalites and trondhjemites occur as blocks within serpentinite or as concordant to crosscutting veins in amphibolite (Lázaro et al. 2009; Blanco-Quintero et al. 2011a) and are interpreted to represent partial melts of subducted basaltic rocks formed at approximately 750 °C and 15 kbar (García-Casco et al. 2008; Lázaro et al. 2009; Blanco-Quintero et al. 2011a, b). As proposed by Cárdenas-Párraga et al. (2012), fluid release from these cooling anatectic melts could have led to crystallization of high-temperature jadeitite in the Sierra del Convento (assumed P-type by the authors, hydrothermal zircon ages: 107.4 ± 0.5, 107.8 ± 1.1 Ma). Because the northern part of Hispaniola was attached to eastern Cuba until the opening of the Cayman Trough in the early Paleogene (e.g., Rosencrantz et al. 1988; Pindell et al. 2006; Pindell and Kennan 2009), rocks now exposed in these Cuban mélanges and the RSJC were in close proximity within the same island arc segment during the Aptian and Albian (e.g., Pindell and Kennan 2009; Boschman et al. 2014). Consequently, the leucocratic rocks which crystallized roughly at the same time as the tonalites/trondhjemites of the eastern Cuban mélanges represent potential jadeitite protoliths, if we consider the spatial proximity within the island arc system, the very similar crystallization ages of jadeitite protoliths and tonalites/trondhjemites, as well as the magmatic arc affinity of the igneous zircon from jadeite rocks. However, the presence of *old* (~117 Ma) igneous zircon and *young* metamorphic zircon domains (~78 Ma) in the concordant jadeitite layer would imply a long residence time of protolith/jadeitite at high-pressure metamorphic conditions inside the subduction zone.

Another possibility is the crystallization of protoliths close to a mid-ocean ridge in the Colombian Marginal Seaway or the Proto-Caribbean, where sea-floor spreading was active from ~150 Ma and lasted until Maastrichtian time (71 Ma, Pindell and Kennan, 2009, and references therein). As discussed in the previous section, zircon crystallized in partial melts of the lower oceanic crust may yield trace-element values similar to those of the igneous zircon separated from the jadeite rocks of this study (Grimes et al. 2015). The formation of jadeitite precursor rocks might have also occurred in a suprasubduction-zone setting, analogous to a petrogenetic model for felsic lithologies exposed in the Oman-UAE Ophiolite (phase 2 magmatism, Goodenough et al. 2014, and references therein). During incipient subduction of warm oceanic lithosphere, slab-derived melts could have intruded the hanging wall of the subducting Proto-Caribbean slab and crystallized, for example, as a gabbro-trondhjemite association that might subsequently had been integrated into the trench and transformed into blueschist and jadeite-rich rocks.

REE patterns and oxygen isotopes of zircon from jadeitites worldwide

Figure 8c–e shows REE patterns of zircon from additional jadeitite localities. Igneous zircons, as defined by the respective authors from the Myanmar (Yui et al. 2013), Tone (Yui et al. 2012) and Osayama (Fu et al. 2010) jadeitites, possess REE patterns that are very similar to those of zircon from oceanic plagiogranites (Grimes et al. 2009). One notable deviation from plagiogranite-like patterns is given by the missing negative Eu anomaly in zircon from the Myanmar jadeitite (Fig. 8c). Metamorphic zircon may be clearly distinct from igneous zircon, such as in the case of the Myanmar jadeitite, or show only slightly depleted REE values relative to the respective igneous zircon domains (Tone and Osayama jadeitites). The metamorphic zircon domains of the *young* age group from the concordant jadeitite layer (30046) share the general REE characteristics with the metamorphic domains from the Myanmar jadeitites.

The $\delta^{18}O$(Zrn) values obtained from the *young* zircon domains (metamorphic) of sample 30046 are higher than the values of corresponding *old* (igneous) domains (Fig. 9a), while metamorphic zircon domains from the Osayama jadeitites possess lower $\delta^{18}O$(Zrn) values than the respective core domains (Fig. 9b). This supports the observations of Fu et al. (2010, 2013) that igneous zircons have mantle-like values of $\delta^{18}O$ (4.7–5.9 ‰), whereas metamorphic zircons re-equilibrated with, were replaced by, or grew in metamorphic fluids/melts with highly variable $\delta^{18}O$(Zrn) ratios. Consequently, $\delta^{18}O$ values of zircon formed during jadeitite formation or metamorphism may be highly variable, e.g., depending on the source of the zircon-forming fluid (Rubatto and Angiboust 2015), but very likely distinct from uniformly mantle-like ratios of igneous zircon from igneous oceanic rocks (Grimes et al. 2011, 2013). Moreover, Fu et al. (2010) determined the oxygen isotope ratios of zircon from the Guatemala (South of Motagua Fault Zone, sample MVE02-8-6 of Flores et al. 2013) and Syros jadeitites (Fig. 9b). Among other things, the primitive, mantle-like $\delta^{18}O$(Zrn) ratios served as strong evidence that all zircon from the Syros sample and many from the Guatemala jadeitite are likely of igneous origin.

Figure 8f shows the average shape of chondrite-normalized REE patterns of zircon from selected Guatemala jadeitites analyzed by Flores et al. (2013) using in situ SHRIMP-RG measurements of zircon-rich fragments of thin sections or polished rock sections. This method preserves valuable information about the host minerals of zircon, but element concentrations are only accurate when

the beam size does not exceed the size of the zircon grains that are available in the respective section (Flores et al. 2013). Some zircon REE patterns shown in Fig. 8f exhibit positive Ce and negative Eu anomalies, but, despite sample MVE02-8-6, REE concentrations are depleted relative to zircon from igneous oceanic rocks (Flores et al. 2013). Flores et al. (2013) interpreted all of the zircon as "having a syn-crystallization hydrothermal origin," mainly based on (1) zircon morphology and the distribution of zircon within the thin section and (2) the occurrence of primary mineral and fluid inclusions in zircon grains that were interpreted to be primary. As a consequence, all the jadeitites, including sample MVE02-8-6, are considered to be fluid precipitates (P-type). However, zircon from at least one sample (MVE02-8-6) of Flores et al. (2013) possesses geochemical and oxygen isotope (Fu et al. 2010) values that are typical for zircon from igneous oceanic rocks and, moreover, lack primary inclusions of jadeite (Flores et al. 2013; see their Table 1). It is therefore plausible that some zircon grains from this particular sample are also igneous as proposed by Fu et al. (2010).

Jadeite inclusions in zircon as unequivocal evidence for P-type formation of jadeitites?

Primary jadeite inclusions in zircon, i.e., jadeite entrapment during zircon growth, would serve as a strong argument for a metamorphic origin of the respective zircon grain and connect the zircon growth to jadeitite genesis (e.g., Fu et al. 2010). Vice versa, inclusions of typical igneous minerals are consistent with igneous zircon and, when found in jadeitites, represent convincing evidence for a metasomatic origin of the particular jadeitite sample (Mori et al. 2011; Yui et al. 2012). However, while the primary relationship between igneous inclusions and zircon is often undisputed (type of mineral and lack of it in the rock matrix), it is usually difficult to prove whether jadeite inclusions in the zircon are primary or not. Careful inspection of zircon textures by high-resolution imaging is needed, because jadeite may have formed along cracks or replaced igneous mineral inclusions after the zircon had already grown (e.g., Fu et al. 2010). The fissures that would allow fluids to migrate into the zircon grain may lie perpendicular to the plane of the thin section or the polished surface of the sample mount, making it difficult to decide whether inclusions are primary or secondary. Such fissures may also have healed subsequent to growth of the "inclusion." The lawsonite inclusion in igneous zircon from the blueschist (30045) of this study (see Fig. 6a, grain no. 6) is an excellent example for such a secondary inclusion, sometimes also called a "pseudo-inclusion" (e.g., Gebauer et al. 1997; Zhang et al. 2009).

Schertl et al. (2012) initially suggested that zircon in the phengite-rich jadeitite (30071) is metamorphic, and the age of the zircon was interpreted to reflect the crystallization age of the phengite-rich jadeitite. Similar to Flores et al. (2013), Schertl et al. (2012) based their interpretation mainly on the occurrence of jadeite and omphacite inclusions that, in the case of sample 30071, mimic the chemical composition of jadeite in the rock matrix. However, REE patterns and Th/U ratios actually call for an igneous origin of the zircon in sample 30071, and indeed, the age of the zircon cores of about 114 Ma is intriguingly similar to the protolith ages of the other jadeite rocks investigated here (113–117 Ma). Considering these new data, it is more likely that the jadeite inclusions in zircon from the phengite-rich jadeitite (30071) are secondary. Consequently, this zircon age is now suggested to represent the age of protolith formation rather than the age of jadeitite crystallization.

Jadeite inclusions in zircon are often considered to be the crucial factor for the decision whether zircon grains in jadeitites are igneous or metamorphic because geochemical signatures such as Th/U ratios and REE patterns alone are not unequivocal proof for the mode of zircon formation (Harley et al. 2007). Therefore, we suggest that, if an interpretation is mainly based upon mineral inclusions in zircon, the inclusions and the textures of enclosing zircons have to be sufficiently documented since an adequate documentation is also required for other key (geochemical) evidence. As noted by Rubatto and Hermann (2007), successful interpretation of zircon ages is accomplished best by combining various microanalytical techniques that in the end allow a consistent interpretation of zircon formation. In the case of zircon in jadeitites, determination of oxygen isotope signatures by ion microprobe is a promising additional tool that helps to reliably differentiate between igneous and metamorphic zircon and finally between a metasomatic (R-type) and an hydrothermal (P-type) origin of jadeitite samples.

Conclusions

Thorough interpretation of small-scale observations is a key to understanding large-scale orogenic processes, and both the timing and mode of jadeitite formation have played a role in formulating subduction-zone models (e.g., Tsujimori and Harlow 2012; Harlow et al. 2015). Here we have documented the nature of individual domains of zircon crystals, which were studied with a combination of various analytical techniques such as SEM-CL, SIMS for U–Pb age, trace elements including REE and oxygen isotope ratios, and EMP of mineral inclusions, to deduce whether jadeite-rich rocks exposed in the northern RSJC represent products of a metasomatic replacement process or formed by direct crystallization from a hydrous fluid.

The jadeite-bearing veins cutting blueschist blocks, with their crack-seal and fissure-growth characteristics (Schertl et al. 2012), would have been the prime target for studying jadeite-rich rocks of very probable P-type origin. Despite considerable effort, no zircon grains were found in any samples of this rock type. We therefore focused on a layer of concordant jadeitite and its host blueschist, as well as on loose blocks of jadeitite and an albite-jadeite rock. The ages of *old* zircon domains from the concordant jadeitite layer are very similar to the ages derived from zircon of the blueschist country rock and the other jadeite-rich samples studied, ranging from 117.1 ± 0.9 Ma to 113.4 ± 1.3 Ma. *Younger* zircon domains found in the concordant jadeitite layer yield 77.6 ± 1.3 Ma, with a poorly defined *intermediate* population ranging from 106 to 90 Ma. A genetic connection is also indicated by similar systematic relationships in the $\delta^{18}O$(Zrn) values. Likewise, the REE patterns of zircon of the different jadeite-rich rocks are nearly identical to the patterns displayed by igneous zircon from rocks of igneous oceanic crust, with the exception of the *younger* zircon domains. Thus, we interpret most of the zircon to have been inherited from an igneous protolith, and all jadeite rocks investigated here are seen as products of metasomatic replacement of pre-existing igneous rocks (R-type). The *younger* ages obtained for zircon from the jadeitite layer (~78 Ma) must be related to a metamorphic event within the Greater Antilles subduction zone, which subducted Proto-Caribbean oceanic crust from at least 120 Ma to approximately 60 Ma (Krebs et al. 2008, 2011; Pindell et al. 2012). P–T conditions conducive to the formation of jadeite-bearing blueschists in the maturing and cooling subduction zone were attained between ~80 and ~60 Ma (Krebs et al. 2008, 2011). The *younger* ~78 Ma ages could be contemporaneous with the metasomatic replacement process that formed the jadeitite, although unequivocal evidence linking zircon and jadeite growth is still missing. We note that these *younger* ages correspond well with the age of metamorphism of various blueschists in the RSJC mélange (Krebs et al. 2008, 2011) ranging from ~80 to ~60 Ma. Based on a worldwide compilation, Tsujimori and Harlow (2012) recently concluded that the age of formation of jadeitite may be significantly older than the peak-metamorphic age of rocks derived and exhumed from the subducted slab. However, in the case of the RSJC mélange, our study shows that this older age does not date the jadeitite formation but instead results from inherited igneous zircon. Yui et al. (2013) came to a similar conclusion for the Myanmar occurrence. Clearly, a critical appraisal of the true significance of zircon ages will be required before such worldwide generalizations can be interpreted.

Our study shows that R-type jadeitite formation is an important and perhaps dominant process in the RSJC mélange. However, P- and R-type processes are probably just end-member scenarios in both space and time in a subduction zone (Yui et al. 2012). Maresch et al. (2012) showed that jadeite could form by both replacement and direct precipitation in the same sample during the course of a metamorphic cycle. The sample of phengite-rich jadeitite (30071) reported on here was shown to have inherited igneous zircon, indicating R-type formation. On the other hand, Schertl et al. (2012) showed that this rock sample also possesses jadeite domains with oscillatory zoning, indicating open-system, P-type direct precipitation.

Acknowledgments The work presented here is part of the PhD thesis of A. Hertwig that was financially supported by Deutsche Forschungsgemeinschaft (SCHE 517/10-1). We are grateful to Peter Segler at the Selfrag Lab and Mineral Processing Laboratories of the TU Bergakademie Freiberg for assistance during zircon separation. We would also like to thank Joe Wooden and other staff of the US Geological Survey–Stanford University Ion Probe Laboratory for assistance during SHRIMP analyses. Comments of Craig Grimes and an anonymous reviewer helped to substantially improve the manuscript. WiscSIMS is partly supported by the US National Science Foundation (EAR 1355590).

References

Amante C, Eakins BW (2009) ETOPO1—1 Arc-Minute Global Relief Model: Procedures, Data Sources and Analysis. NOAA Technical Memorandum NESDIS NGDC-24

Anders E, Grevesse N (1989) Abundances of the elements: meteoritic and solar. Geochim Cosmochim Acta 53(1):197–214. doi:10.1016/0016-7037(89)90286-X

Andres U (2010) Development and prospects of mineral liberation by electrical pulses. Int J Miner Process 97(1–4):31–38. doi:10.1016/j.minpro.2010.07.004

Barth AP, Wooden JL (2006) Timing of magmatism following initial convergence at a passive margin, southwestern US Cordillera, and ages of lower crustal magma sources. J Geol 114:231–245

Barth AP, Wooden JL (2010) Coupled elemental and isotopic analyses of polygenetic zircons from granitic rocks by ion microprobe, with implications for melt evolution and the sources of granitic magmas. Chem Geol 277:149–159

Black LP, Kamo SL, Allen CM, Davis DW, Aleinikoff JN, Valley JW et al (2004) Improved $^{206}Pb/^{238}U$ microprobe geochronology by the monitoring of a trace-element-related matrix effect; SHRIMP, ID-TIMS, ELA-ICP-MS and oxygen isotope documentation for a series of zircon standards. Chem Geol 205:115–140

Blanco-Quintero IF, Rojas-Agramonte Y, García-Casco A, Kröner A, Mertz DF, Lázaro C et al (2011a) Timing of subduction and exhumation in a subduction channel: evidence from slab melts from La Corea Mélange (eastern Cuba). Lithos 127(1–2):86–100. doi:10.1016/j.lithos.2011.08.009

Blanco-Quintero IF, Gerya TV, García-Casco A, Castro A (2011b) Subduction of young oceanic plates: a numerical study with application to aborted thermal-chemical plumes. Geochem Geophys Geosyst. doi:10.1029/2011GC003717

Boschman LM, van Hinsbergen DJJ, Torsvik TH, Spakman W, Pindell JL (2014) Kinematic reconstruction of the Caribbean region since the Early Jurassic. Earth Sci Rev 138:102–136. doi:10.1016/j.earscirev.2014.08.007

Bowman JR, Moser DE, Valley JW, Wooden JL, Kita NT, Mazdab FK (2012) Zircon U-Pb isotope, $\delta^{18}O$ and trace element response to 80 my of high temperature metamorphism in the lower crust: sluggish diffusion and new records of Archean craton formation. Am J Sci 311(9):719–772. doi:10.2475/09.2011.01

Bröcker M, Keasling A (2006) Ionprobe U-Pb zircon ages from the high-pressure/low-temperature mélange of Syros, Greece: age diversity and the importance of pre-Eocene subduction. J Metamorph Geol 24(7):615–631

Cárdenas-Párraga J, García-Casco A, Núñez Cambra K, Rodriguez-Vega A, Blanco Quintero I, Harlow GE, Lázaro C (2010) Jadeitite jade occurrence from the Sierra del Convento mélange (eastern Cuba). Bol Soc Geo Mex 62(1):199–205

Cárdenas-Párraga J, García-Casco A, Harlow GE, Blanco-Quintero IF, Rojas-Agramonte Y, Kröner A (2012) Hydrothermal origin and age of jadeitites from Sierra del Convento Mélange. Eur J Mineral 24(2):313–331. doi:10.1127/0935-1221/2012/0024-2171

Cavosie AJ, Kita NT, Valley JW (2009) Primitive oxygen-isotope ratio recorded in magmatic zircon from the Mid-Atlantic Ridge. Am Mineral 94(7):926–934. doi:10.2138/am.2009.2982

Coleman RG (1977) Ophiolites-Ancient oceanic lithosphere?. Springer, Berlin

Compagnoni R, Rolfo F, Manavella F, Salusso F (2007) Jadeitite in the Monviso meta-ophiolite, Piemonte Zone. Ital West Alps. Period Mineral 76(2–3):79–89

Compagnoni R, Rolfo F, Castelli D (2012) Jadeitite from the Monviso meta-ophiolite, western Alps: occurrence and genesis. Eur J Mineral 24(2):333–342. doi:10.1127/0935-1221/2011/0023-2164

Draper G, Nagle F (1991) Geology, structure and tectonic development of the Rio San Juan Complex, northern Dominican Republic. In: Mann P, Draper G, Lewis JF (eds) Special Paper 262: Geologic and Tectonic Development of the North America-Caribbean Plate Boundary in Hispaniola. Geol Soc Am, Boulder (Colorado), pp 77–95

Escuder-Viruete J (2010) Mapa Geológico de la República Dominica: Hojas de Río San Juan, Guayabito, Salcedo, Gaspar Hernández, Pimentel, Cabrera y Villa Riva. Instituto Geológico y Minero de España, Santo Domingo (R.D.)

Escuder-Viruete J, Pérez-Estaún A (2013) Contrasting exhumation P-T paths followed by high-P rocks in the northern Caribbean subduction-accretionary complex: insights from the structural geology, microtextures and equilibrium assemblage diagrams. Lithos 160–161:117–144. doi:10.1016/j.lithos.2012.11.028

Escuder-Viruete J, Friedman R, Castillo-Carrión M, Jabites J, Pérez-Estaún A (2011) Origin and significance of the ophiolitic high-P mélanges in the northern Caribbean convergent margin: insights from the geochemistry and large-scale structure of the Río San Juan metamorphic complex. Lithos 127(3–4):483–504. doi:10.1016/j.lithos.2011.09.015

Escuder-Viruete J, Valverde-Vaquero P, Rojas-Agramonte Y, Gabites J, Castillo-Carrión M, Pérez-Estaún A (2013a) Timing of deformational events in the Río San Juan complex: implications for the tectonic controls on the exhumation of high-P rocks in the northern Caribbean subduction–accretionary prism. Lithos 177:416–435. doi:10.1016/j.lithos.2013.07.006

Escuder-Viruete J, Valverde-Vaquero P, Rojas-Agramonte Y, Jabites J, Pérez-Estaún A (2013b) From intra-oceanic subduction to arc accretion and arc-continent collision: insights from the structural evolution of the Río San Juan metamorphic complex, northern Hispaniola. J Struct Geol 46:34–56. doi:10.1016/j.jsg.2012.10.008

Ferry JM, Watson EB (2007) New thermodynamic models and revised calibrations for the Ti-in-zircon and Zr-in-rutile thermometers. Contrib Mineral Petrol 154(4):429–437. doi:10.1007/s00410-007-0201-0

Flores KE, Martens UC, Harlow GE, Brueckner HK, Pearson NJ (2013) Jadeitite formed during subduction: in situ zircon geochronology constraints from two different tectonic events within the Guatemala Suture Zone. Earth Planet Sci Lett 371–372:67–81. doi:10.1016/j.epsl.2013.04.015

Floyd PA, Yaliniz MK, Goncuoglu MC (1998) Geochemistry and petrogenesis of intrusive and extrusive ophiolitic plagiogranites, Central Anatolian Crystalline Complex, Turkey. Lithos 42:225–241

Fu B, Mernagh TP, Kita NT, Kemp AI, Valley JW (2009) Distinguishing magmatic zircon from hydrothermal zircon: a case study from the Gidginbung high-sulphidation Au–Ag–(Cu) deposit SE Australia. Chem Geol 259(3–4):131–142. doi:10.1016/j.chemgeo.2008.10.035

Fu B, Valley JW, Kita NT, Spicuzza MJ, Paton C, Tsujimori T, Bröcker M, Harlow GE (2010) Multiple origins of zircons in jadeitite. Contrib Mineral Petrol 159(6):769–780

Fu B, Paul B, Cliff J, Bröcker M, Bulle F (2012) O-Hf isotope constraints on the origin of zircon in high-pressure mélange blocks and associated matrix rocks from Tinos and Syros Greece. Eur J Mineral 24(2):277–287. doi:10.1127/0935-1221/2011/0023-2131

Fu B, Kita NT, Wilde SA, Liu X, Cliff J, Greig A (2013) Origin of the Tongbai-Dabie-Sulu Neoproterozoic low-$\delta^{18}O$ igneous province, east-central China. Contrib Mineral Petrol 165(4):641–662. doi:10.1007/s00410-012-0828-3

García-Casco A, Lázaro C, Rojas-Agramonte Y, Kröner A, Torres-Roldán RL, Núñez Cambra K et al (2008) Partial melting and counterclockwise P-T path of subducted oceanic crust (Sierra del Convento Melange, Cuba). J Petrol 49(1):129–161

García-Casco A, Rodriguez-Vega A, Cárdenas-Párraga J, Iturralde-Vinent MA, Lázaro C, Blanco Quintero I, Rojas-Agramonte Y, Kröner A, Núñez Cambra K, Millan G, Torres-Roldán RL, Carrasquilla S (2009) A new jadeitite jade locality (Sierra del Convento, Cuba): first report and some petrological and archeological implications. Contrib Mineral Petrol 158(1):1–16

Gebauer D, Schertl H, Brix M, Schreyer W (1997) 35 Ma old ultrahigh-pressure metamorphism and evidence for very rapid exhumation in the Dora Maira Massif, Western Alps. Lithos 41:5–24

Geisler T, Schaltegger U, Tomaschek F (2007) Re-equilibration of Zircon in aqueous fluids and melts. Elements 3(1):43–50. doi:10.2113/gselements.3.1.43

Goodenough KM, Thomas RJ, Styles MT, Schofield DI, MacLeod CJ (2014) Records of Ocean growth and destruction in the Oman-UAE Ophiolite. Elements 10(2):109–114. doi:10.2113/gselements.10.2.109

Grimes CB, John BE, Kelemen PB, Mazdab FK, Wooden JL, Cheadle MJ, Hanghøj K, Schwartz JJ (2007) Trace element chemistry of zircons from oceanic crust: a method for distinguishing detrital zircon provenance. Geol 35(7):643–646. doi:10.1130/G23603A.1

Grimes CB, John BE, Cheadle MJ, Mazdab FK, Wooden JL, Swapp S, Schwartz JJ (2009) On the occurrence, trace element geochemistry, and crystallization history of zircon from in situ ocean lithosphere. Contrib Mineral Petrol 158(6):757–783. doi:10.1007/s00410-009-0409-2

Grimes CB, Ushikubo T, John BE, Valley JW (2011) Uniformly mantle-like $\delta^{18}O$ in zircons from oceanic plagiogranites and gabbros. Contrib Mineral Petrol 161(1):13–33

Grimes CB, Ushikubo T, Kozdon R, Valley JW (2013) Perspectives on the origin of plagiogranite in ophiolites from oxygen isotopes in zircon. Lithos 179:48–66. doi:10.1016/j.lithos.2013.07.026

Grimes CB, Wooden JL, Cheadle MJ, John BE (2015) "Fingerprinting" tectono-magmatic provenance using trace elements in igneous zircon. Contrib Mineral Petrol 170:46. doi:10.1007/s00410-015-1199-3

Harley SL, Kelly NM, Möller A (2007) Zircon behaviour and the thermal histories of mountain chains. Elements 3(1):25–30. doi:10.2113/gselements.3.1.25

Harlow GE (1994) Jadeitites, albitites and related rocks from the Motagua Fault Zone Guatemala. J Metamorph Geol 12(1):49–68

Harlow GE, Sorensen SS (2005) Jade (Nephrite and Jadeitite) and Serpentinite: metasomatic connections. Int Geol Rev 47(2):113–146

Harlow GE, Sorensen SS, Sisson VB (2007) Jade Deposits. In: Groat LA (ed) Geology of Gem Deposits, 1st edn., Quebec, pp 207–254

Harlow GE, Sisson VB, Sorensen SS (2011) Jadeitite from Guatemala: new observations and distinctions among multiple occurrences. Geol Acta 9(3–4):363–387

Harlow GE, Tsujimori T, Sorensen SS (2015) Jadeitites and plate tectonics. Annu Rev Earth Pl Sci 43:105–138. doi:10.1146/annurev-earth-060614-105215

Hertwig A (2014) Genesis of jadeitites and their country rocks, Rio San Juan Complex, Dominican Republic. PhD Dissertation, 1-382, Ruhr-Universität Bochum

Hoskin PW (2005) Trace-element composition of hydrothermal zircon and the alteration of Hadean zircon from the Jack Hills Australia. Geochim Cosmochim Acta 69(3):637–648. doi:10.1016/j.gca.2004.07.006

Hoskin PW, Black LP (2000) Metamorphic zircon formation by solid-state recrystallization of protolith igneous zircon. J Metamorph Geol 18:423–439

Hoskin WO, Schaltegger U (2003) The composition of zircon and Igneous and Metamorphic Petrogenesis. In: Hanchar JM, Hoskin WO (eds) Zircon. Mineralogical Society of America; Geochemical Society, Washington (D.C.), vol. 53, pp 27–55

Kita NT, Ushikubo T, Fu B, Valley JW (2009) High precision SIMS oxygen isotope analysis and the effect of sample topography. Chem Geol 264:43–57

Koepke J, Feig ST, Snow J, Freise M (2004) Petrogenesis of oceanic plagiogranites by partial melting of gabbros: an experimental study. Contrib Mineral Petrol 146(4):414–432. doi:10.1007/s00410-003-0511-9

Koepke J, Berndt J, Feig ST, Holtz F (2007) The formation of SiO_2-rich melts within the deep oceanic crust by hydrous partial melting of gabbros. Contrib Mineral Petrol 153(1):67–84. doi:10.1007/s00410-006-0135-y

Korotev RL (1996) A self-consistent compilation of elemental concentration data for 93 geochemical reference samples. Geostand Geoanal Res 20(2):217–245. doi:10.1111/j.1751-908X.1996.tb00185.x

Krebs M (2008) Druck-Temperatur-Zeit-Pfade subduktionszonenbezogener Hochdruckmetamorphite des Rio San Juan-Komplexes, Dominikanische Republik. PhD Dissertation, Bd. I, 1-443, Bd. II, 1-419, Ruhr-Universität Bochum

Krebs M, Maresch WV, Schertl H, Münker C, Baumann A, Draper G, Idleman B, Trapp E (2008) The dynamics of intra-oceanic subduction zones: a direct comparison between fossil petrological evidence (Rio San Juan Complex, Dominican Republic) and numerical simulation. Lithos 103(1–2):106–137. doi:10.1016/j.lithos.2007.09.003

Krebs M, Schertl H, Maresch WV, Draper G (2011) Mass flow in serpentinite-hosted subduction channels: P–T–t path patterns of metamorphic blocks in the Rio San Juan mélange (Dominican Republic). J Asian Earth Sci 42(4):569–595. doi:10.1016/j.jseaes.2011.01.011

Lázaro C, García-Casco A, Agramonte YR, Kröner A, Neubauer F, Iturralde-Vinent MA (2009) Fifty-five-million-year history of oceanic subduction and exhumation at the northern edge of the Caribbean plate (Sierra del Convento mélange, Cuba). J Metamorph Geol 27(1):19–40

Liati A, Gebauer D, Fanning C (2004) The age of ophiolitic rocks of the Hellenides (Vourinos, Pindos, Crete): first U-Pb ion microprobe (SHRIMP) zircon ages. Chem Geol 207(3–4):171–188. doi:10.1016/j.chemgeo.2004.02.010

Ludwig KR (2001) Squid version 1.02: a users manual, vol 2. Berkeley Geochronological Center Special Publications, Berkeley, pp 1–22

Ludwig KR (2003) Mathematical-Statistical Treatment of Data and Errors for ^{230}Th/U Geochronology. Rev Mineral Geochem 52:631–656

Ludwig KR (2012) User's manual for isoplot 3.75: a geochronological toolkit for microsoft excel, vol 5. Berkeley Geochronological Center Special Publications, Berkeley, pp 1–75

Mann P, Draper G, Lewis JF (1991) An overview of the geologic and tectonic development of Hispaniola. In: Mann P, Draper G, Lewis JF (eds) Special paper 262: geologic and tectonic development of the North America-Caribbean plate boundary in Hispaniola. Geological Society of America, Boulder (Colorado), pp 1–28

Maresch WV, Grevel C, Stanek KP, Schertl H, Carpenter MA (2012) Multiple growth mechanisms of jadeite in Cuban metabasite. Eur J Mineral. doi:10.1127/0935-1221/2012/0024-2179

Mattinson JM (2010) Analysis of the relative decay constants of ^{235}U and ^{238}U by multi-step CA-TIMS measurements of closed-system natural zircon samples. Chem Geol 275(3–4):186–198

Mattinson CG, Wooden JL, Zhang JX, Bird DK (2009) Paragneiss zircon geochronology and trace element geochemistry, North Qaidam HP/UHP terrane, western China. J Asian Earth Sci 35(3–4):298–309. doi:10.1016/j.jseaes.2008.12.007

Mazdab FK (2009) Characterization of flux-grown Trace-element-doped titanite using the high-mass-resolution ion microprobe (SHRIMP-RG). Can Mineral 47(4):813–831. doi:10.3749/canmin.47.4.813

Mazdab FK, Wooden J (2006) Trace element analysis in zircon by ion microprobe (SHRIMP-RG): technique and applications. Geochim Cosmochim Acta 70(18):A405. doi:10.1016/j.gca.2006.06.817

McClelland WC, Gilotti JA, Mazdab FK, Wooden JL (2009) Trace-element record in zircons during exhumation from UH*P* conditions North-East Greenland Caledonides. Eur J Mineral 21(6):1135–1148. doi:10.1127/0935-1221/2009/0021-2000

Meng F, Makeyev AB, Yang J (2011) Zircon U-Pb dating of jadeitite from the Syum-Keu ultramafic complex, Polar Urals, Russia: constraints for subduction initiation. J Asian Earth Sci 42(4):596–606. doi:10.1016/j.jseaes.2011.01.013

Meng F, Yang H-J, Makeyev AB, Ren Y, Kulikova KV, Bryanchaninova NI (2016) Jadeitite in the Syum-Keu ultramafic complex from Polar Urals, Russia: insights into fluid activity in subduction zones. Eur J Mineral (in press)

Mori Y, Orihashi Y, Miyamoto T, Shimada K, Shigeno M, Nishiyama T (2011) Origin of zircon in jadeitite from the Nishisonogi metamorphic rocks, Kyushu Japan. J Metamorph Geol 29(6):673–684. doi:10.1111/j.1525-1314.2011.00935.x

Page FZ, Fu B, Kita NT, Fournelle J, Spicuzza MJ, Schulze DJ, Viljoen F, Basei MA, Valley JW (2007a) Zircons from kimberlite: new insights from oxygen isotopes, trace elements, and Ti in zircon thermometry. Geochim Cosmochim Acta 71(15):3887–3903. doi:10.1016/j.gca.2007.04.031

Page FZ, Ushikubo T, Kita NT, Riciputi LR, Valley JW (2007b) High-precision oxygen isotope analysis of picogram samples reveals 2 micron gradients and slow diffusion in zircon. Am Mineral 92(10):1772–1775. doi:10.2138/am.2007.2697

Pindell J, Kennan L (2009) Tectonic evolution of the Gulf of Mexico, Caribbean and northern South America in the mantle reference frame: an update. In: James KH, Lorente MA, Pindell J (eds) Special Publications 328: The Origin and Evolution of the Caribbean Plate. Geological Society, London, pp 1–55

Pindell J, Kennan L, Stanek KP, Maresch WV, Draper G (2006) Foundations of Gulf of Mexico and Caribbean evolution: eight controversies resolved. Geol Acta 4(1–2):303–341

Pindell J, Maresch WV, Martens UC, Stanek KP (2012) The Greater Antillean Arc: early Cretaceous origin and proposed relationship to Central American subduction mélanges: implications for models of Caribbean evolution. Int Geol Rev 54(2):131–143. doi:10.1080/00206814.2010.510008

Qiu Z, Wu F, Yang S, Zhu M, Sun J, Yang P (2009) Age and genesis of the Myanmar jadeite: constraints from U–Pb ages and Hf isotopes of zircon inclusions. Chin Sci Bull 54(4):658–668. doi:10.1007/s11434-008-0490-3

Rosencrantz E, Ross MI, Sclater JG (1988) Age and spreading history of the Cayman Trough as determined from depth, heat flow, and magnetic anomalies. J Geophys Res 93(B3):2141–2157. doi:10.1029/JB093iB03p02141

Rubatto D (2002) Zircon trace element geochemistry: partitioning with garnet and the link between U–Pb ages and metamorphism. Chem Geol 184(1–2):123–138. doi:10.1016/S0009-2541(01)00355-2

Rubatto D, Angiboust S (2015) Oxygen isotope record of oceanic and high-pressure metasomatism. A P–T–time–fluid path for the Monviso eclogites (Italy). Contrib Mineral Petrol. doi:10.1007/s00410-015-1198-4

Rubatto D, Hermann J (2003) Zircon formation during fluid circulation in eclogites (Monviso, Western Alps): implications for Zr and Hf budget in subduction zones. Geochim Cosmochim Acta 67(12):2173–2187. doi:10.1016/S0016-7037(02)01321-2

Rubatto D, Hermann J (2007) Zircon behaviour in deeply subducted rocks. Elements 3(1):31–35. doi:10.2113/gselements.3.1.31

Schaltegger U (1999) Growth, annealing and recrystallization of zircon and preservation of monazite in high-grade metamorphism: conventional and in situ U-Pb isotope, cathodoluminescence and microchemical evidence. Contrib Mineral Petrol 134(2–3):186–201

Schertl H, Maresch WV, Stanek KP, Hertwig A, Krebs M, Baese R, Sergeev SS (2012) New occurrences of jadeitite, jadeite quartzite and jadeite-lawsonite quartzite in the Dominican Republic, Hispaniola: petrological and geochronological overview. Eur J Mineral 24(2):199–216. doi:10.1127/0935-1221/2012/0024-2201

Shi G, Cui W, Cao S, Jiang N, Jian P, Liu D, Miao L, Chu B (2008) Ion microprobe zircon U–Pb age and geochemistry of the Myanmar jadeitite. J Geol Soc London 165:221–234

Stacey JA, Kramers JD (1975) Approximation of terrestrial lead isotope evolution by a two-stage model. Earth Planet Sci Lett 26:207–221

Tsujimori T, Harlow GE (2012) Petrogenetic relationships between jadeitite and associated high-pressure and low-temperature metamorphic rocks in worldwide jadeitite localities: a review. Eur J Mineral 24(2):371–390. doi:10.1127/0935-1221/2012/0024-2193

Tsujimori T, Wooden J, Miyamoto T (2005) U-Pb dating of large zircons in low-temperature jadeitite from the Osayama serpentinite melange, Southwest Japan: insights into the timing of serpentinization. Int Geol Rev 47(10):1048–1057

Valley JW (2003) Oxygen isotopes in Zircon. In: Hanchar JM, Hoskin WO (eds) Zircon mineralogical society of America, vol 53. Geochemical Society, Washington (D.C.), pp 343–385

Valley JW, Kita NT (2009) In situ oxygen isotope geochemistry by ion microprobe. In: Fayek M (ed) Secondary Ion Mass Spectrometry in the Earth Sciences, vol 41. Mineralogical Society of Canada, Toronto, pp 19–63

Valley JW, Kinny PD, Schulze DJ, Spicuzza MJ (1998) Zircon megacrysts from kimberlite: oxygen isotope variability among mantle melts. Contrib Mineral Petrol 133:1–11

Valley JW, Bindeman IN, Peck WH (2003) Empirical calibration of oxygen isotope fractionation in zircon. Geochim Cosmochim Acta 67(17):3257–3266. doi:10.1016/S0016-7037(03)00090-5

Valley JW, Lackey JS, Cavosie AJ, Clechenko CC, Spicuzza MJ, Basei MAS, Bindeman IN, Ferreira VP, Sial AN, King EM, Peck WH, Sinha AK, Wei CS (2005) 4.4 billion years of crustal maturation: oxygen isotope ratios of magmatic zircon. Contrib Mineral Petrol 150(6):561–580. doi:10.1007/s00410-005-0025-8

van der Wielen KP, Pascoe R, Weh A, Wall F, Rollinson G (2013) The influence of equipment settings and rock properties on high voltage breakage. Miner Eng 46–47:100–111. doi:10.1016/j.mineng.2013.02.008

Williams IS (1998) U-Pb by ion microprobe. In: McKibben MA, Shanks WC, Ridley WI (eds) Applications of microanalytical techniques to understanding mineralizing processes, vol 7. Society of Economic Geologists, Littleton, pp 1–35

Yui T, Maki K, Usuki T, Lan C, Martens UC, Wu C, Wu T, Liou JG (2010) Genesis of Guatemala jadeitite and related fluid characteristics: insight from zircon. Chem Geol 270(1–4):45–55

Yui T, Kenshi M, Wang K, Lan C, Usuki T, Lizuka Y, Wu C, Wu T, Nishiyama T, Martens UC, Liou JG, Grove M (2012) Hf isotope and REE compositions of zircon from jadeitite (Tone, Japan and north of the Motagua fault, Guatemala): implications on jadeitite genesis and possible protoliths. Eur J Mineral 24(2):263–275. doi:10.1127/0935-1221/2011/0023-2127

Yui T, Fukuyama M, Lizuka Y, Wu C, Wu T, Liou JG, Grove M (2013) Is Myanmar jadeitite of Jurassic age? A fiction from incompletely recrystallized inherited zircon. Lithos 160–161:268–282

Zhang Z, Schertl H, Wang JL, Shen K, Liou JG (2009) Source of coesite inclusions within inherited magmatic zircon from Sulu UHP rocks, eastern China, and their bearing for fluid-rock interaction and SHRIMP dating. J Metamorph Geol 27(4):317–333. doi:10.1111/j.1525-1314.2009.00819.x